



A plasma membrane transporter coordinates phosphate reallocation and grain filling in cereals

Bin Ma^{1,2,3,9}, Lin Zhang^{4,9}, Qifei Gao^{ID 5,6,9}, Junmin Wang^{7,9}, Xiaoyuan Li^{1,2}, Hu Wang², Yu Liu⁸, Hui Lin^{1,2}, Jiyun Liu², Xin Wang², Qun Li², Yiwen Deng², Weihua Tang^{ID 2,✉}, Sheng Luan^{ID 6,✉} and Zuhua He^{ID 1,2,✉}

Phosphate (Pi) is essential to plant growth and crop yield. However, it remains unknown how Pi homeostasis is maintained during cereal grain filling. Here, we identified a rice grain-filling-controlling PHO1-type Pi transporter, OsPHO1;2, through map-based cloning. Pi efflux activity and its localization to the plasma membrane of seed tissues implicated a specific role for OsPHO1;2 in Pi reallocation during grain filling. Indeed, Pi over-accumulated in developing seeds of the *Ospho1;2* mutant, which inhibited the activity of ADP-glucose pyrophosphorylase (AGPase), important for starch synthesis, and the grain-filling defect was alleviated by overexpression of AGPase in *Ospho1;2*-mutant plants. A conserved function was recognized for the maize transporter ZmPHO1;2. Importantly, ectopic overexpression of OsPHO1;2 enhanced grain yield, especially under low-Pi conditions. Collectively, we discovered a mechanism underlying Pi transport, grain filling and P-use efficiency, providing an efficient strategy for improving grain yield with minimal P-fertilizer input in cereals.

Grain filling is a rate-limiting step for grain production in cereal crops such as rice and maize¹. Grain filling is defined by the process by which fertilized ovaries acquire carbohydrate and other nutrients to synthesize starch and convert themselves into caryopses or grains². Several key genes affecting grain filling were identified in rice and maize. For example, *GIF1* and *ZmSweet4c* (*OsSweet4*) show the signature of domestication selection^{3,4}, indicating that grain filling is an important trait coupled with human demands. *GIF1* encodes a cell-wall invertase required for carbon partitioning during the early grain-filling stage⁵. *OsSweet4* encodes a hexose transporter acting downstream of *GIF1* to sustain endosperm development⁴. During grain filling, Pi homeostasis is critical not only because ATP, nucleic acids and phospholipids are critical to central metabolism of seed development but, more importantly, because Pi participates in starch synthesis directly. After transport into the endosperm, glucose and fructose are catalyzed into glucose-1-P (G-1-P) and glucose-6-P with a requirement for Pi as a substrate. G-1-P and ATP are then converted into ADP-glucose (ADP-Glc) and inorganic pyrophosphate (PPi) by AGPase^{5,6}. While ADP-Glc is directly used for starch synthesis, PPi is hydrolyzed to Pi by inorganic pyrophosphatase⁵. As a rate-limiting enzyme in starch synthesis, the activity of AGPase is activated by 3-phosphoglycerate and inhibited by Pi through an allosteric mechanism⁷. In addition to starch synthesis, glucose-6-P can also participate in the synthesis of phytic acid, which accounts for 65–80% of total P in seeds^{8,9}. Therefore, grain filling is tightly coupled with Pi utilization and storage, rendering Pi homeostasis critical for grain filling and crop yield. However, little is known about the mechanism of Pi homeostasis during seed development.

In cereal plants, soluble Pi is taken up from the soil by roots that transfer Pi to above-ground tissues, and it is ultimately loaded into

seeds during grain filling. A number of Pi transporters are responsible for sequential steps of Pi uptake and translocation in rice¹⁰. The OsPHT1 family consists of 13 members that are localized to the plasma membrane and function in Pi uptake into the cell as assayed in heterologous systems including yeast and *Xenopus* oocytes^{11–17}. Many of the identified OsPHT1 transporters are highly expressed in roots under normal or P-deficient conditions to facilitate both acquisition and translocation of Pi in rice^{10,11,15}. The PHO1 family of Pi transporters was shown to function in root-to-shoot Pi distribution in *Arabidopsis*¹⁸. There are three PHO1 members in rice¹⁹, among which OsPHO1;2 is the only one proposed to be responsible for translocation of Pi from root to shoot²⁰. However, the transporter activity of OsPHO1;2 and its paralogs have not been determined. Concerning Pi transport from source to sink tissues, PHT1-type transporters OsPT4 and OsPT8 play an important role in Pi distribution from roots and leaves to seeds. While OsPT4 loads Pi into the embryo¹², OsPT8 loads Pi from the panicle axis to the hull during seed development¹⁶. Disrupting OsPT4 or OsPT8 results in yield decrease^{12,16}, suggesting that source-to-sink translocation of Pi is indispensable for seed development. In addition, two rice sulfate transporters, OsSULTR3;3 and SPDT, appear to play a role in controlling P content in seeds^{21,22}. In particular, SPDT is highly expressed in the node and is likely the major transporter responsible for allocation of leaf Pi to the seed²².

Seed development requires a large Pi supply, but excessive Pi levels can be harmful. How do plants strike a balance between Pi supply and demand? This should be determined by the control of both Pi influx and efflux. However, little is known about mechanisms of Pi homeostasis and reallocation during seed development. In this study, we identified that a frame-shift mutation in the OsPHO1;2 gene was responsible for the grain-filling defect in a rice mutant.

¹School of Life Science and Technology, ShanghaiTech University, Shanghai, China. ²National Key Laboratory of Plant Molecular Genetics, CAS Center for Excellence in Molecular Plant Sciences, Institute of Plant Physiology & Ecology, Chinese Academy of Sciences, Shanghai, China. ³University of the Chinese Academy of Sciences, Beijing, China. ⁴Co-Innovation Center for Modern Production Technology of Grain Crops, Yangzhou University, Yangzhou, China. ⁵School of Life Sciences, Northwest University, Xi'an, China. ⁶Department of Plant and Microbial Biology, University of California, Berkeley, CA, USA. ⁷Institute of Crops and Nuclear Technology Utilization, Zhejiang Academy of Agricultural Sciences, Hangzhou, China. ⁸State Key Laboratory of Rice Biology, Institute of Crop Sciences, Zhejiang University, Hangzhou, China. ⁹These authors contributed equally: Bin Ma, Lin Zhang, Qifei Gao, Junmin Wang.
✉e-mail: whtang@cemps.ac.cn; sluan@berkeley.edu; zhhe@cemps.ac.cn

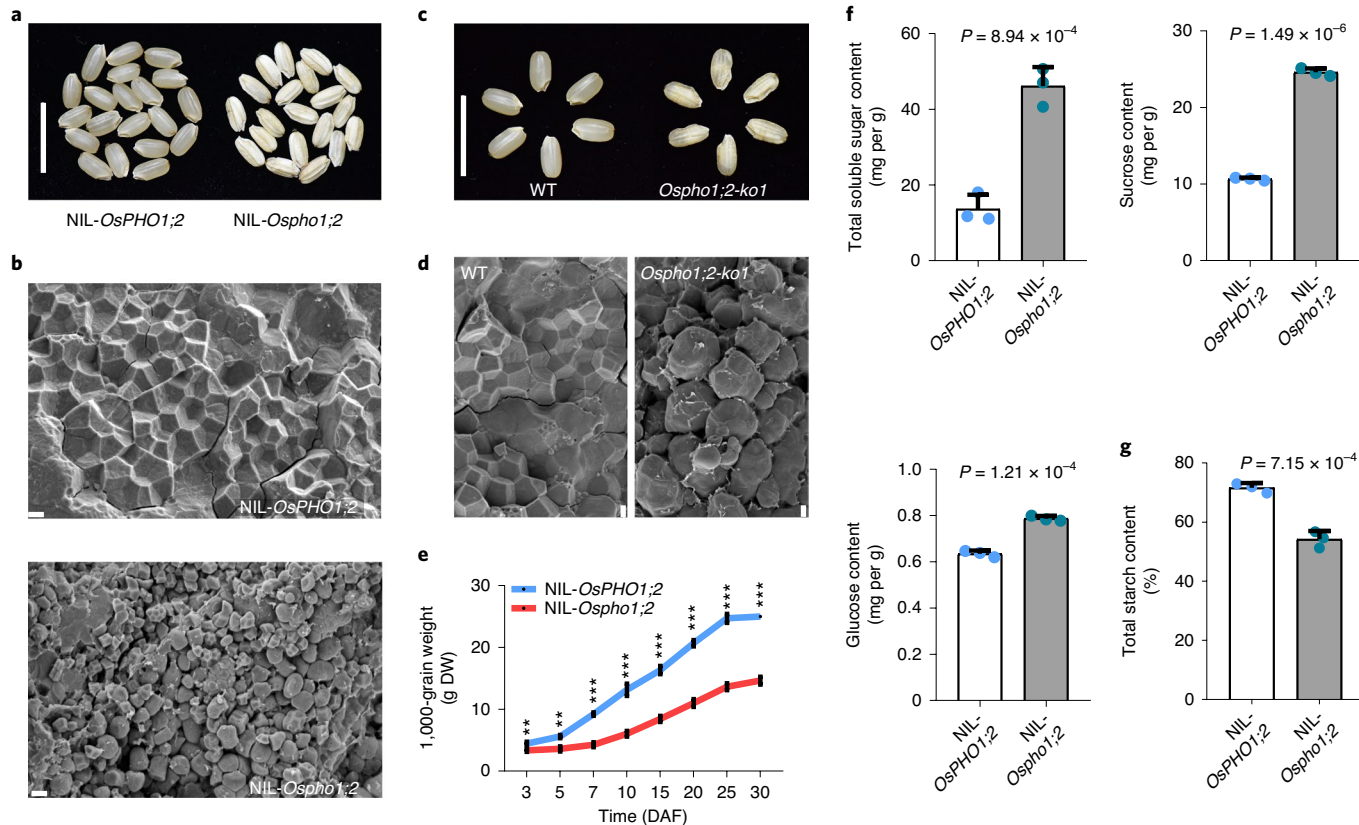


Fig. 1 | Characteristics of the *Ospho1;2* mutant with incomplete grain filling. **a**, Seed phenotypes of NIL-OsPHO1;2 and NIL-Ospho1;2 plants. **b**, Field emission scanning electron microscopic images of seed cross-sections from NIL-OsPHO1;2 and NIL-Ospho1;2 plants at the mature stage. **c**, Seed phenotypes of WT and CRISPR-Cas9 knockout allele 1 (*Ospho1;2-ko1*) plants. **d**, Field emission scanning electron microscopic images of seed cross-sections from WT and *Ospho1;2-ko1* plants. **e**, Comparison of the grain-filling rate from 3 to 30 DAF between NIL-OsPHO1;2 and NIL-Ospho1;2 plants. Values are mean \pm s.d. ($n=3$ plants); ** $P < 0.01$, *** $P < 0.001$ by two-tailed Student's *t*-tests. $P = 9.26 \times 10^{-3}$, $P = 2.31 \times 10^{-3}$, $P = 6.40 \times 10^{-5}$, $P = 3.71 \times 10^{-4}$, $P = 7.90 \times 10^{-5}$, $P = 3.30 \times 10^{-5}$, $P = 3.00 \times 10^{-5}$, $P = 1.00 \times 10^{-5}$, respectively (3–30 DAF). DW, dry weight. **f**, Measurements of total soluble sugar content, sucrose content and glucose content. Values are mean \pm s.d. ($n=3$ plants). **g**, Measurement of total starch content. Values are mean \pm s.d. ($n=3$ plants). P values are indicated, calculated by two-tailed Student's *t*-tests (**f,g**). Scale bars, 1 cm (**a,c**) and 2 μ m (**b,d**). Independent experiments were repeated two times with similar results (**b,e–g**).

We show that OsPHO1;2 primarily mediates Pi efflux to facilitate Pi unloading from the endosperm of developing seeds, which is critical for starch synthesis during grain filling. We also found that the maize ortholog encoding ZmPHO1;2 functions similarly in seed development. Thus, we identified a plant Pi efflux transporter that functions in Pi reallocation essential for starch biosynthesis during cereal grain filling, providing new insight into Pi homeostasis and recycling in plants as well as a new crop-breeding target for improvement of yield and P-use efficiency (PUE) for sustainable agriculture.

Results

Phenotypes and map-based cloning of the grain-filling mutant *Ospho1;2*. From our breeding stock collection, we identified a naturally occurring mutant with a poor grain-filling phenotype. The defective phenotype was controlled by a single recessive locus initially mapped to a ~370-kb region on chromosome 2 (Extended Data Fig. 1a). To facilitate phenotype evaluation, a pair of near-isogenic lines (NILs) were developed and named NIL-OsPHO1;2 and NIL-Ospho1;2 after gene cloning (see below). NIL-Ospho1;2 seeds showed typical grain-filling defects with loosely and irregularly packed starch granules, leading to thin and shrunken grains and severe yield loss. The mutant plants were otherwise normal except for reduced tiller number (Fig. 1a,b and Extended Data Fig. 2a–i). The 1,000-grain weight was reduced by almost half throughout

seed development in NIL-Ospho1;2 plants (Fig. 1e). Different from *gif1*-mutant plants, another grain-filling mutant previously described²³, NIL-Ospho1;2 plants contained less starch and more soluble sugars and were more resistant to bacterial blight (Fig. 1f,g and Extended Data Fig. 2j). This indicated that *Ospho1;2* affects different physiological processes.

Using the NIL population, we confined the mutation to a ~5-kb region in which we identified a single gene, *LOC_Os02g56510* (Extended Data Fig. 1b). This candidate gene encodes a putative Pi transporter of the PHO1 family, namely OsPHO1;2 (ref.²⁰). To identify the causal mutation in NIL-Ospho1;2, we sequenced the 5-kb region and found a 1-bp deletion in exon 7 of *OsPHO1;2*, leading to a frame shift and premature termination in the coding sequence. We also identified two synonymous SNPs in exon 1 and exon 3 and one SNP in intron 12 (Extended Data Fig. 3a). To confirm whether the OsPHO1;2 mutation was responsible for the defective grain-filling phenotype, we generated eight CRISPR-Cas9 knockout (ko) lines, *Ospho1;2-ko1* to *Ospho1;2-ko8*, in Nipponbare (NIP) (Extended Data Fig. 3b), which all showed the same grain-filling defects as NIL-Ospho1;2 plants (Fig. 1c,d and Extended Data Fig. 3c–i), and ectopic overexpression of the full-length coding sequence (CDS) of OsPHO1;2 complemented the grain-filling phenotype of *Ospho1;2-ko1* plants (Supplementary Fig. 1a–f). Together, these results link the function of OsPHO1;2 to grain filling in rice.

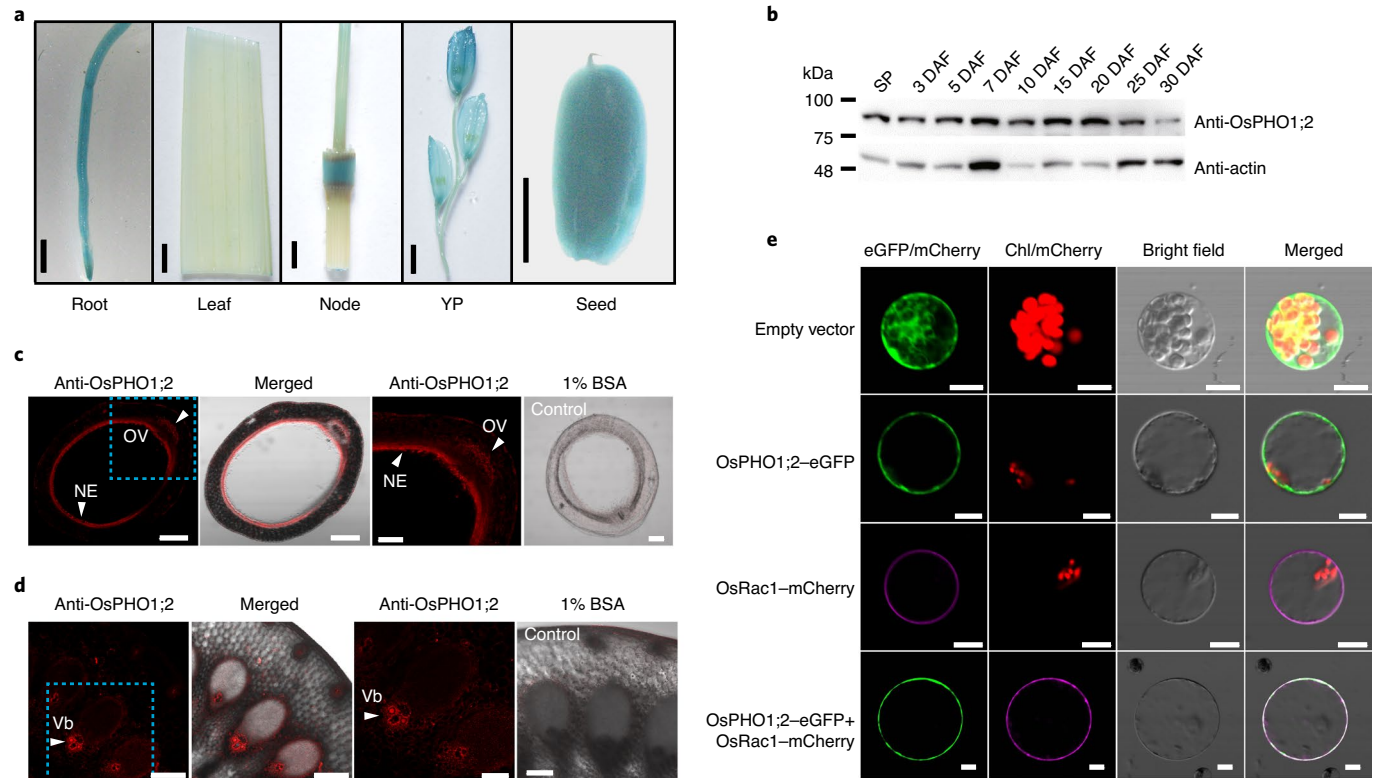


Fig. 2 | OsPHO1;2 is a plasma membrane protein with tissue-specific expression. **a**, Expression pattern of *OsPHO1;2*, as revealed by the GUS fusion reporter. *OsPHO1;2* was highly expressed in the root, node, young panicle (YP) and developing grain. Scale bars, 3 mm. **b**, Protein level of *OsPHO1;2* at the grain-filling stage, immunodetected with an anti-*OsPHO1;2* antibody by western blotting, with total proteins extracted from dehulled seeds at the indicated times. Actin was detected as a loading control. SP, spikelet. **c,d**, Tissue specificity of *OsPHO1;2* expression in early-filling grains at 5 DAF (**c**) and in node I (**d**), revealed by in situ immunofluorescence in WT (NIP) plants. Images are representative of three replicates. White arrowheads indicate the NE, OV and vascular bundles (Vb). Images in blue boxes are magnified on the right. Scale bars, 200 μ m (left) and 100 μ m (right). Samples incubated with 1% BSA were used as negative controls. Independent experiments were repeated two times with similar results (**b-d**). **e**, Plasma membrane localization of *OsPHO1;2* in the rice protoplast. *OsPHO1;2* was colocalized with the plasma membrane-localized GTPase *OsRac1*. Images are representative of six independent cells. Scale bars, 10 μ m. eGFP, enhanced GFP; chl, chloroplast.

OsPHO1;2 is a plasma membrane protein highly expressed in developing seeds. In addition to expression in the young panicle, hull and roots, *OsPHO1;2* was also highly expressed in developing seeds as revealed by quantitative reverse-transcription PCR (qRT-PCR) (Extended Data Fig. 4a). This expression pattern was confirmed by histological analysis of the *pOsPHO1;2*- β -glucuronidase (GUS) reporter in transgenic plants (Fig. 2a). Consistently, the *OsPHO1;2* protein was enriched in grains during the entire filling stages from 0 d after flowering (DAF) (spikelets) to 30 DAF and in the nodes (Fig. 2b and Extended Data Fig. 4b). To further investigate the cell specificity of *OsPHO1;2*, immunofluorescence assays with an anti-*OsPHO1;2* antibody were performed in seeds and node I at the early grain-filling stage. Interestingly, a strong fluorescence signal was detected in the nuellar epidermis (NE) and ovular vasculature (OV) of the seed, from which cells function in loading and unloading nutrients to and from the endosperm^{3,24} (Fig. 2c). Fluorescent signals were also found in vascular bundles of node I (Fig. 2d), which contribute to nutrient distribution in the rice plant^{25,26}. We further validated the expression of *OsPHO1;2* in different tissues of developing seeds and found that both *OsPHO1;2* mRNA and the *OsPHO1;2* protein could be detected in the embryo, endosperm, pericarp and NE (Extended Data Fig. 4c,d). In addition, the localization of *OsPHO1;2* in the seed was further validated using transgenic lines harboring a *pOsPHO1;2*-GUS reporter (Extended Data Fig. 4e,f).

Subcellular localization is critical for the function of a transporter. Delivering a construct to transiently express green fluorescent protein (GFP) fused to *OsPHO1;2* into rice sheath protoplasts and onion epidermal cells, we found that, in both cases, *OsPHO1;2*-GFP was mainly localized in the plasma membrane (Fig. 2e and Supplementary Fig. 2a,b). A weak fluorescence signal was occasionally observed inside the cell, suggesting that a portion of *OsPHO1;2* proteins might be localized in intracellular compartments (Supplementary Fig. 2a). To further confirm its function in grain filling, we generated stable transgenic lines that overexpressed the *OsPHO1;2*-GFP fusion protein driven by the maize ubiquitin promoter and found that GFP signals were mainly localized at the plasma membrane of endosperm cells in developing seeds (Supplementary Fig. 3). We then performed immunoelectron microscopy analysis to further clarify the subcellular localization of *OsPHO1;2*. We found that immunogold particles were associated with the plasma membrane of cells from the NE and vascular bundles (Extended Data Fig. 5a-f). In sum, these results indicate that *OsPHO1;2* is a plasma membrane-localized protein and is highly expressed in the NE and vascular tissues of developing seeds.

OsPHO1;2 is a Pi transporter primarily mediating Pi efflux. There has been no direct evidence that plant PHO1-type proteins, such as *OsPHO1;2*, function as Pi transporters. It is also notable that, although *Osmo1;2* seedlings were smaller than wild-type (WT)

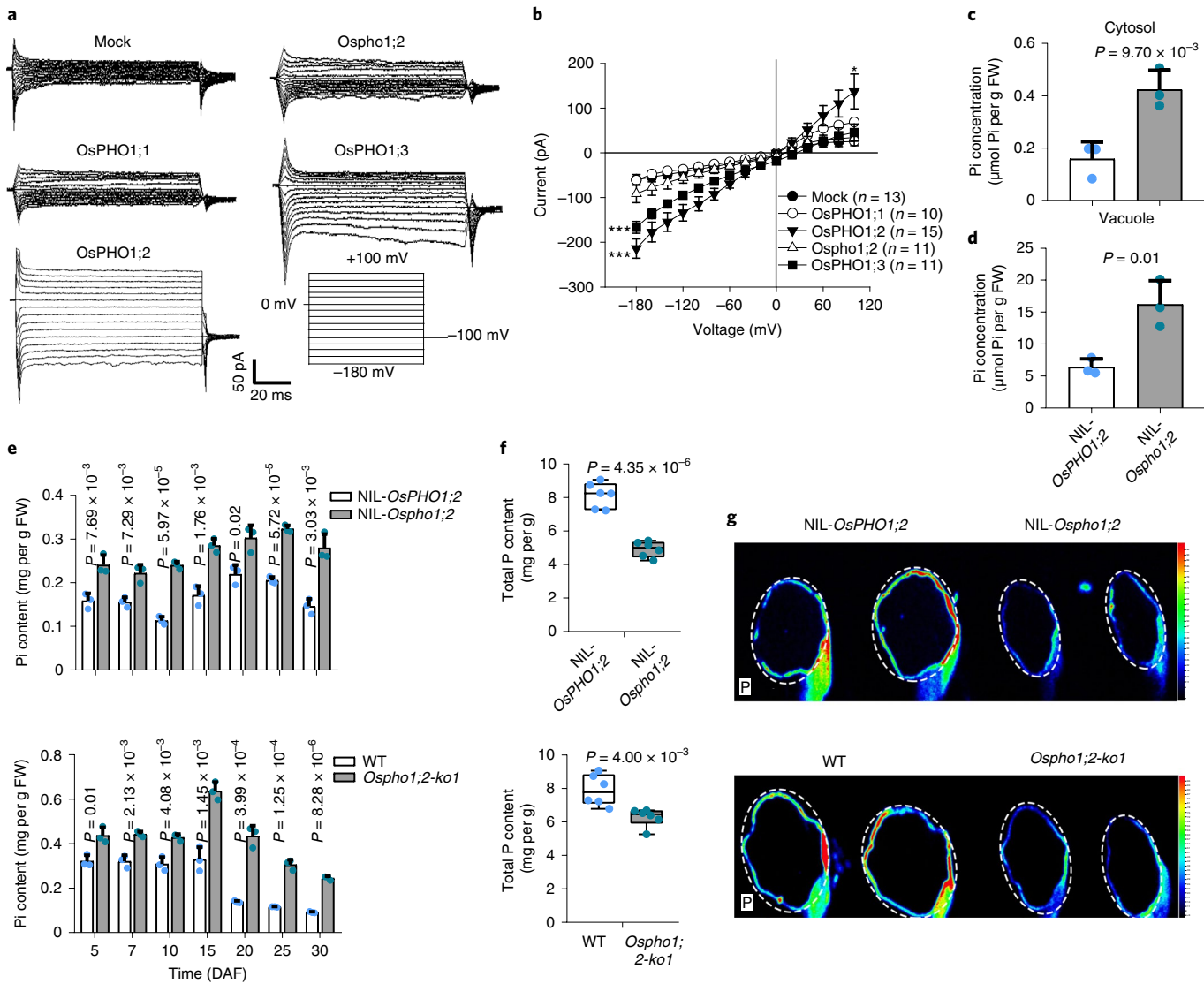


Fig. 3 | Patch-clamp recording of transporter activity and analysis of Pi and total P content. **a**, Typical whole-cell recordings of mammalian HEK293T cells expressing OsPHO1;1, OsPHO1;2, Ospho1;2, OsPHO1;3 and a mock control. **b**, Average current-voltage curves for cells expressing OsPHO1;1, OsPHO1;2, Ospho1;2, OsPHO1;3 and the mock control. Error bars depict mean \pm s.e.m., and the exact mammalian cell number (n) is indicated on the graph. * $P < 0.05$, ** $P < 0.001$ by two-tailed Student's *t*-tests. OsPHO1;2 at +100 mV, $P = 0.015$; OsPHO1;2 at -180 mV, $P = 2.73 \times 10^{-6}$; OsPHO1;3 at -180 mV, $P = 5.54 \times 10^{-6}$. **c,d**, Quantification of Pi in the cytosol (**c**) and vacuole (**d**) in NIL-OsPHO1;2 and NIL-Ospho1;2 seedling roots by *in vivo* proton-decoupled ^{31}P NMR. Values are mean \pm s.d. ($n=3$ plants). FW, fresh weight. **e**, Measurement of Pi content in dehulled seeds at the grain-filling stage. Grains from NILs (top) and WT and Ospho1;2-ko1 plants (bottom) at 5–30 DAF were compared; values are mean \pm s.d. ($n=3$ biologically independent samples). **f**, Measurement of total P content in NILs and WT and Ospho1;2-ko1 brown rice ($n=6$ plants). For box-and-whisker plots, the central line, box and whiskers indicate the median, interquartile range (IQR) and 1.5 times the IQR, respectively. **g**, Total P distribution in NILs and WT and Ospho1;2-ko1 brown rice, imaged with a μ XRF spectrometer. Normalized X-ray fluorescence intensities are scaled from red (maximum) to blue (minimum) as indicated at the right, and two seeds of each line are shown. Actual seed areas are circled with white dashed lines. P values are indicated according to two-tailed Student's *t*-tests (**c–f**).

seedlings during the early growth stage²⁰ (~5 weeks under our field conditions), possibly due to less energy supplied from the defective endosperm, they later resumed a WT stature (Extended Data Fig. 2a,e). These growth dynamics suggested that OsPHO1;2 may not be required for overall plant growth and development but is indispensable for grain filling. To dissect the mechanism underlying the function of OsPHO1;2 in grain filling and Pi homeostasis, we sought to determine whether the OsPHO1;2 protein indeed functions as a Pi transporter using three different heterologous expression systems. First, we showed that OsPHO1;2 complemented the growth phenotype of the yeast mutant EY917 (ref. ²⁷), which lacks five Pi transporters

(*pho84Δ*, *pho87Δ*, *pho89Δ*, *pho90Δ*, *pho91Δ*) responsible for Pi uptake (Supplementary Fig. 4), providing evidence that OsPHO1;2 may have Pi transport activity. Furthermore, we used patch-clamp recording to examine the Pi transport activity mediated by three OsPHO1-type proteins when expressed in the mammalian cell line HEK293T (Methods). Results indicated that OsPHO1;2 was active in mediating both Pi influx and efflux and that the efflux activity was predominant, while the mutated Ospho1;2 protein lost Pi transport activity in both directions (Fig. 3a,b). Our results also showed that OsPHO1;1 and OsPHO1;3 were less active than OsPHO1;2 (Fig. 3a,b). In addition, we tested the transport activity of the three

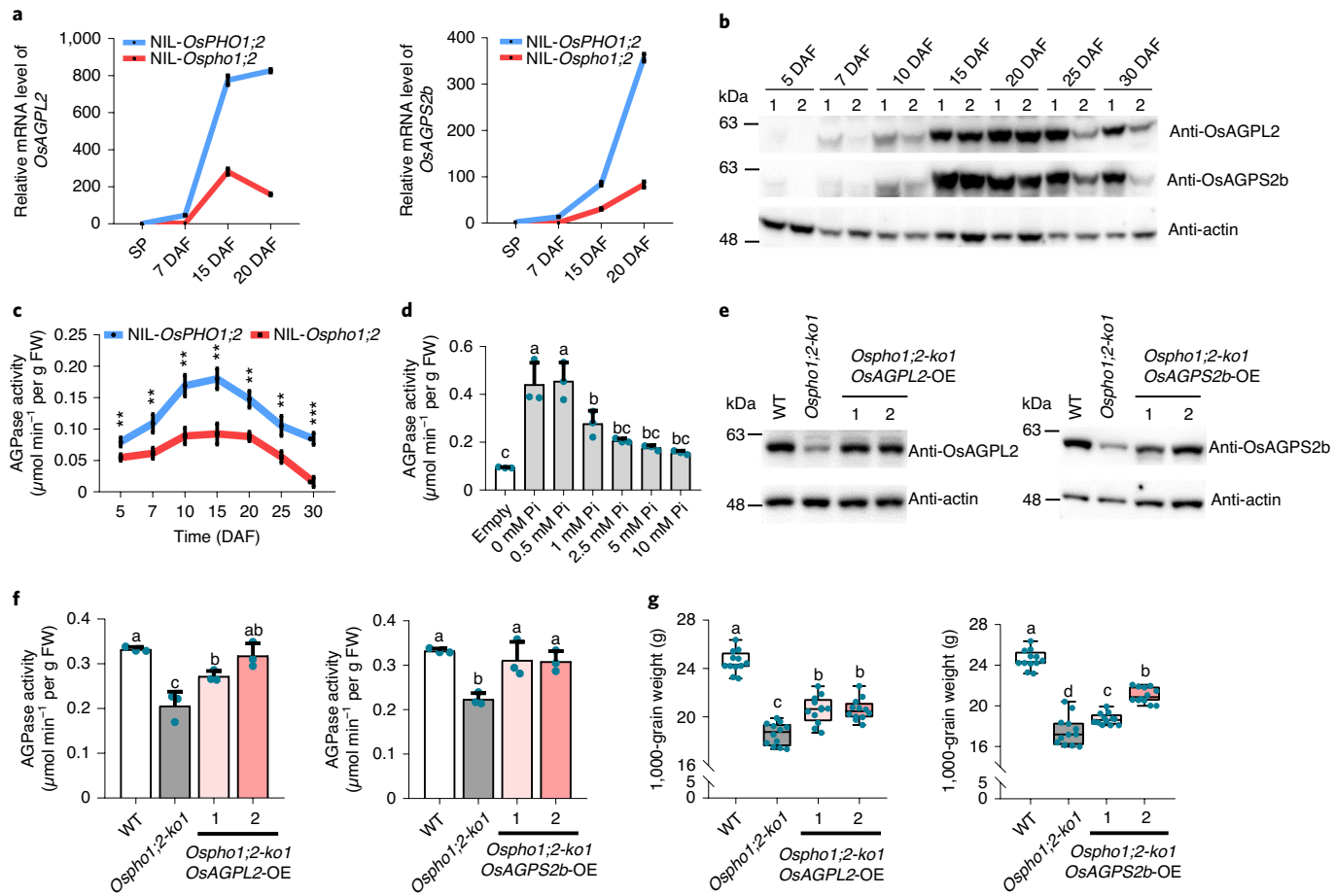


Fig. 4 | AGPase activity is inhibited by Pi accumulation, and its ectopic overexpression can partially rescue the grain-filling defect of the *Ospho1;2* mutant. **a**, mRNA levels of AGPase genes at the filling stage were quantified by qRT-PCR and normalized to the rice *Actin* gene. Values are mean \pm s.d. ($n=3$ technical repeats). **b**, Protein levels of OsAGPL2 and OsAGPS2b in dehulled seeds from NILs at the filling stage, detected by western blotting. Actin was used as a loading control. Numbers 1 and 2 represent NIL-OsPHO1;2 and NIL-Ospho1;2 samples, respectively. **c**, Measurement of AGPase activity in NILs at the grain-filling stage from 5 to 30 DAF. Values are mean \pm s.d. ($n=3$ biologically independent samples). Independent experiments were repeated at least two times with similar results. ** $P < 0.01$, *** $P < 0.001$ by two-tailed Student's *t*-tests. $P = 8.88 \times 10^{-3}$, $P = 8.86 \times 10^{-3}$, $P = 3.10 \times 10^{-3}$, $P = 3.03 \times 10^{-3}$, $P = 2.65 \times 10^{-3}$, $P = 9.84 \times 10^{-3}$, $P = 7.31 \times 10^{-4}$, respectively (5–30 DAF). **d**, In vitro Pi inhibition of AGPase activity produced in *E. coli*. Values are mean \pm s.d. ($n=3$ independent cell cultures). $P = 1.50 \times 10^{-6}$ by one-way ANOVA. **e**, Protein levels of OsAGPL2 and OsAGPS2b in WT and *Ospho1;2-ko1* plants and two ectopic overexpression lines by western blotting. Actin was used as a loading control. Note that overexpression of OsAGPL2 and OsAGPS2b largely restored their levels in the OsPHO1;2-knockout background. **f**, Measurement of AGPase activity at the grain-filling stage in *Ospho1;2-ko1* seeds ectopically overexpressing OsAGPL2 and OsAGPS2b. Values are mean \pm s.d. ($n=3$ biologically independent samples). OsAGPL2-OE, $P = 4.54 \times 10^{-4}$; OsAGPS2b-OE, $P = 3.12 \times 10^{-3}$ by one-way ANOVA. **g**, Grain weights of OsAGPL2 and OsAGPS2b ectopic overexpression lines in the OsPHO1;2-knockout background ($n=12$ plants). For box-and-whisker plots, the central line, box and whiskers indicate the median, IQR and 1.5 times the IQR, respectively. OsAGPL2-OE, $P = 7.29 \times 10^{-18}$; OsAGPS2b-OE, $P = 2.98 \times 10^{-21}$ by one-way ANOVA. Different letters at the top of each column indicate a significant difference at $P < 0.05$, determined by Tukey's honest significant differences (HSD) test (**d,f,g**).

OsPHO1 proteins in *Xenopus* oocytes over a pH gradient (pH 5.5, 6.5 and 7.5) and confirmed that OsPHO1;2 showed strong Pi transport activity that was not altered by pH values, suggesting that OsPHO1;2 may not transport Pi by a proton symport (Extended Data Fig. 6a–f). It is noteworthy that Pi efflux activity represents a primary function of this transporter because the plasma membrane potential is normally in the -100-mV range in most plant cells under physiological conditions. These patch-clamping analyses provide direct evidence demonstrating the transport activity of PHO1-type proteins in plants. The predominant efflux activity may mediate xylem Pi loading, thus explaining the previous genetic analysis showing their functions in root-to-shoot Pi transfer^{20,28}.

To link the function of OsPHO1;2 in Pi transport to Pi homeostasis, we compared Pi levels among seedlings of NILs. When grown

either under Pi starvation or with a normal Pi supply, mutant plants showed increased Pi content in the roots but decreased Pi content in the shoots (Extended Data Fig. 7a,b). Therefore, the OsPHO1;2 mutation impaired root-to-shoot transfer of Pi, consistent with previous results²⁰. Further, ^{31}P NMR analysis revealed that both cytosolic and vacuolar Pi contents were notably higher in the root cells of mutant seedlings, excluding the possibility of OsPHO1;2 being involved in the cytosol–vacuole partition (Fig. 3c,d). Next, we examined Pi distribution in above-ground tissues at the mature stage and found that both NIL-Ospho1;2 and *Ospho1;2-ko1* plants had higher Pi content than WT plants in nodes, husks and brown rice but showed lower levels in leaves (Extended Data Fig. 7c,d), suggesting that OsPHO1;2 may be involved in reallocation of Pi between seeds and leaves. In support of this hypothesis, we measured

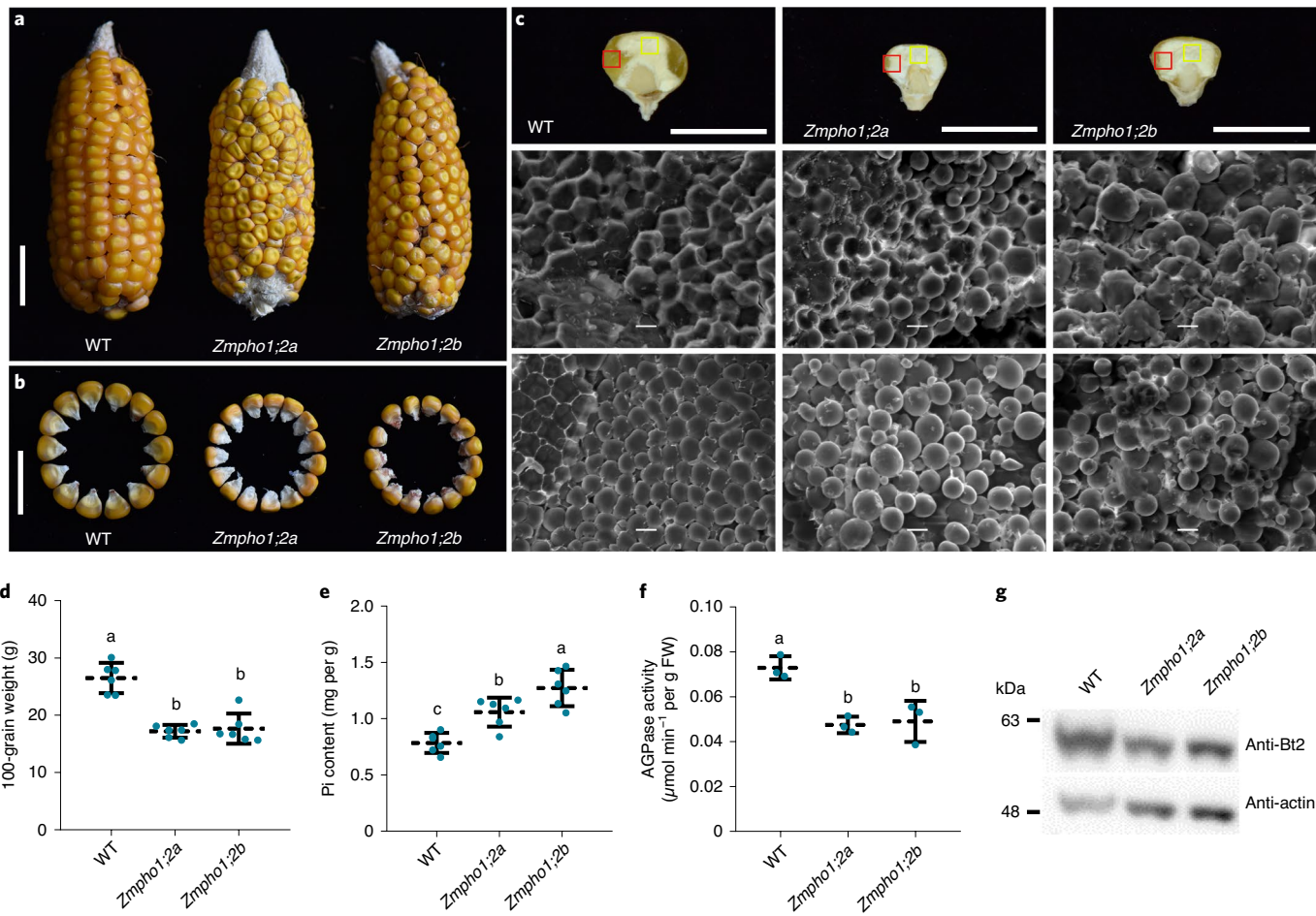


Fig. 5 | ZmPHO1;2 also participates in Pi homeostasis and grain filling. **a,b**, Ear (**a**) and kernel (**b**) morphology of *ZmPHO1;2*-knockout mutants, *Zmpho1;2a* and *Zmpho1;2b* mutants and WT plants. Scale bars, 2 cm. **c**, Scanning electron microscopic images of starch granules from WT and *Zmpho1;2a*- and *Zmpho1;2b*-mutant plants. Top, kernel transverse sections; scale bars, 1 cm. Middle, scanning electron microscopic images of kernel peripheral regions indicated by the red boxes on the kernels. Bottom, scanning electron microscopic images of kernel central regions indicated by the yellow boxes. Scale bars, 10 μ m. **d–f**, Comparisons of 100-grain weight (**d**), Pi content at the mature stage (**e**) and AGPase activity at 18 DAF (**f**) in WT, *Zmpho1;2a*- and *Zmpho1;2b*-mutant grains. Values are mean \pm s.d. ($n=6$ plants for **d,e**; $n=3$ biologically independent samples for **f**). $P=3.35\times 10^{-6}$ (**d**), $P=4.17\times 10^{-5}$ (**e**), $P=4.79\times 10^{-3}$ (**f**) by one-way ANOVA. Different letters indicate a significant difference at $P<0.05$, determined by Tukey's HSD test. **g**, Protein level of the maize AGPase Bt2 decreased in filling kernels of maize *ZmPHO1;2*-knockout mutants, as revealed by western blotting. Actin was used as a loading control. Independent experiments were repeated two times with similar results (**c,g**).

Pi levels in developing seeds and found higher Pi content in the mutant throughout grain filling (Fig. 3e). As OsPHO1;2 is highly expressed in NE tissues of developing seeds, we compared Pi content in the endosperm and pericarp that surround the NE and found that Pi content in these tissues was significantly increased in NIL-*Osmpho1;2* seeds (Extended Data Fig. 7e). Therefore, Pi reallocation from developing seeds was disturbed in *Osmpho1;2* mutants. However, the total P content was greatly reduced in mutant seeds (Fig. 3f), and consistent results were observed in images obtained by micro X-ray fluorescence (μ XRF) (Fig. 3g). This suggests that synthesis of organic P compounds might be decreased in mutant plants due to the disruption of Pi exchange between maternal and filial tissues in the seed. We thus conclude that OsPHO1;2 functions as a Pi efflux transporter that unloads Pi from endosperm cells, and its loss of function leads to Pi excess in the seed.

Excess Pi accumulation inhibits starch-synthesis enzymes. To assess the relationship between Pi accumulation and grain filling, we performed a comparative RNA-seq analysis of NILs at the

grain-filling stage, and a large number of differentially expressed genes were identified. We found that many genes involved in starch and sugar metabolism were enriched (Supplementary Fig. 5). Furthermore, we confirmed the expression pattern of several representative genes related to starch synthesis by qRT-PCR, including those encoding AGPase, starch synthase, starch-branched enzyme and starch-debranching enzyme²⁹ (Fig. 4a and Supplementary Fig. 6a–k). Most of these genes were downregulated in the *Osmpho1;2* mutant, consistent with its defects in starch synthesis. As revealed by immunoblotting and isozyme analysis, either the protein level or the enzyme activity of several key enzymes involved in starch synthesis was also decreased in mutant seeds (Fig. 4b and Supplementary Fig. 7a–c). Among these enzymes, AGPase catalyzes the first committed step of starch synthesis to generate ADP-Glc and PPi from G-1-P and ATP, and dysfunction of AGPase was shown to cause grain-filling defects similar to those found in the *Osmpho1;2* mutant³⁰, suggesting an indispensable role in grain filling. It is well established that AGPase enzyme activity is repressed by excess Pi accumulation through a feedback mechanism^{7,31,32}.

AGPase consists of two cytoplasm-localized subunits in rice endosperm³⁰, namely OsAGPL2 and OsAGPS2b, and mRNA levels for both were greatly decreased in the *OspHO1;2* mutant (Fig. 4a). It was observed that AGPase expression was inhibited by high Pi levels³². To establish a possible link between Pi content and AGPase mRNA production, we developed suspension cell culture lines from the NILs and measured AGPase mRNA levels with different Pi levels in the medium. In both cell lines, OsAGPL2 and OsAGPS2b mRNA levels decreased upon exposure to excessive Pi levels in the medium (Extended Data Fig. 8a,b). Together with the fact that both the mRNA level and the activity of AGPase are inhibited by high Pi levels, we speculated that AGPase might serve as a major effector for OsPHO1;2-mediated grain filling. To test this hypothesis, we measured AGPase activity during grain filling from 3 to 30 DAF and found lower enzyme activity associated with NIL-*OspHO1;2* and *OspHO1;2-ko1* plants, correlating with elevated Pi levels in mutant grains (Figs. 3e and 4c and Extended Data Fig. 8c). We also confirmed that the activity of AGPase expressed in *Escherichia coli* was indeed directly inhibited by high concentrations of Pi (Fig. 4d). In summary, we found that excessive Pi levels had a negative impact on both the mRNA level and activity of AGPase, which may underlie reduced starch synthesis and defective grain filling in the *OspHO1;2* mutant.

To further address the causal relationship between decreased AGPase activity and the grain-filling defect, we ectopically overexpressed OsAGPL2 and OsAGPS2b, driven by the maize ubiquitin promoter in the *OspHO1;2-ko1* background. Two homozygous lines overexpressing each transgene with restored protein level relative to the WT were selected for experiments (Fig. 4e). We found that AGPase activity in AGPase-overexpressing (OE) *OspHO1;2-ko1* lines was lower than that in the WT but higher than that in the *OspHO1;2-ko1* mutant (Fig. 4f). After harvest, we observed a partial rescue of grain-filling defects in both AGPase-OE *OspHO1;2-ko1* lines, and overexpression of either OsAGPL2 or OsAGPS2b led to significant increases in 1,000-grain weight (Fig. 4g and Supplementary Fig. 8a-d). Thus, these results further support the notion that OsPHO1;2 sustains grain filling by maintaining proper levels of AGPase activity.

ZmPHO1;2 functions in grain filling and Pi reallocation in maize. Other cereal crops, such as maize, wheat and sorghum, also have PHO1 homologs (Extended Data Fig. 9a). There are two homologs of OsPHO1;2 in maize, namely *ZmPHO1;2a* (*Zm00001d051945*) and *ZmPHO1;2b* (*Zm00001d018445*). To assess whether these maize PHO1-type Pi transporters function in the same manner as OsPHO1;2 in rice, we generated CRISPR-Cas9 knockout mutants in *ZmPHO1;2a* and *ZmPHO1;2b* (Extended Data Fig. 9b) and found that these mutants produced smaller kernels with typical grain-filling defects, including reduced kernel thickness (Fig. 5a,b) and loosely

and irregularly packed starch granules in mutant grains (Fig. 5c). Consequently, the mutant 100-kernel weight was significantly reduced by ~35% compared to that of the WT (Fig. 5d), indicating that *ZmPHO1;2* exerted a similar function during grain filling in maize. Further analyses of AGPase activity and Pi content revealed lower AGPase activity and higher Pi content in developing seeds from *ZmPHO1;2a* and *ZmPHO1;2b* plants (Fig. 5e,f). Moreover, the Bt2 protein (AGPase in maize) was also downregulated in filling kernels from *ZmPHO1;2a*- and *ZmPHO1;2b*-mutant plants (Fig. 5g). We thus conclude that *PHO1;2* genes in maize share a conserved function in grain filling similar to that in rice. In sum, we propose that PHO1;2 is a Pi transporter that plays a key role in Pi homeostasis and reallocation during grain filling of cereal crops.

Ectopic overexpression of *OsPHO1;2* improves grain yield and PUE. To explore the potential of *OsPHO1;2* in rice improvement, we developed transgenic plants ectopically overexpressing *OsPHO1;2* driven by the 35S promoter (*OsPHO1;2-OE*) (Extended Data Fig. 10a), and three independent transgenic lines and one transgene-negative WT line were chosen for further experiments. *OsPHO1;2-OE* plants displayed similar overall morphological traits as compared to those of the WT but showed stronger plant stature with larger panicles and heavier grains than the WT (Fig. 6a,b and Extended Data Fig. 10b-f). Importantly, *OsPHO1;2-OE* lines consistently showed reduced Pi accumulation and increased AGPase protein levels and total enzyme activity in developing seeds (Fig. 6c,d). When Pi content was measured in different tissues, ectopic overexpression lines had lower Pi levels in brown rice and node I but increased Pi levels in the flag leaf (Fig. 6d and Extended Data Fig. 10g). In developing seeds, Pi content in the endosperm was lower in *OsPHO1;2-OE* lines than that in the WT (Extended Data Fig. 10g). Therefore, ectopic overexpression of *OsPHO1;2* may cause enhanced Pi export from seeds, consistent with the function of this transporter. Consequently, total P levels in ectopically overexpressing seeds also decreased (Fig. 6e). These results suggest that increased levels of *OsPHO1;2* activity enhance recycling of Pi from seeds to source tissues.

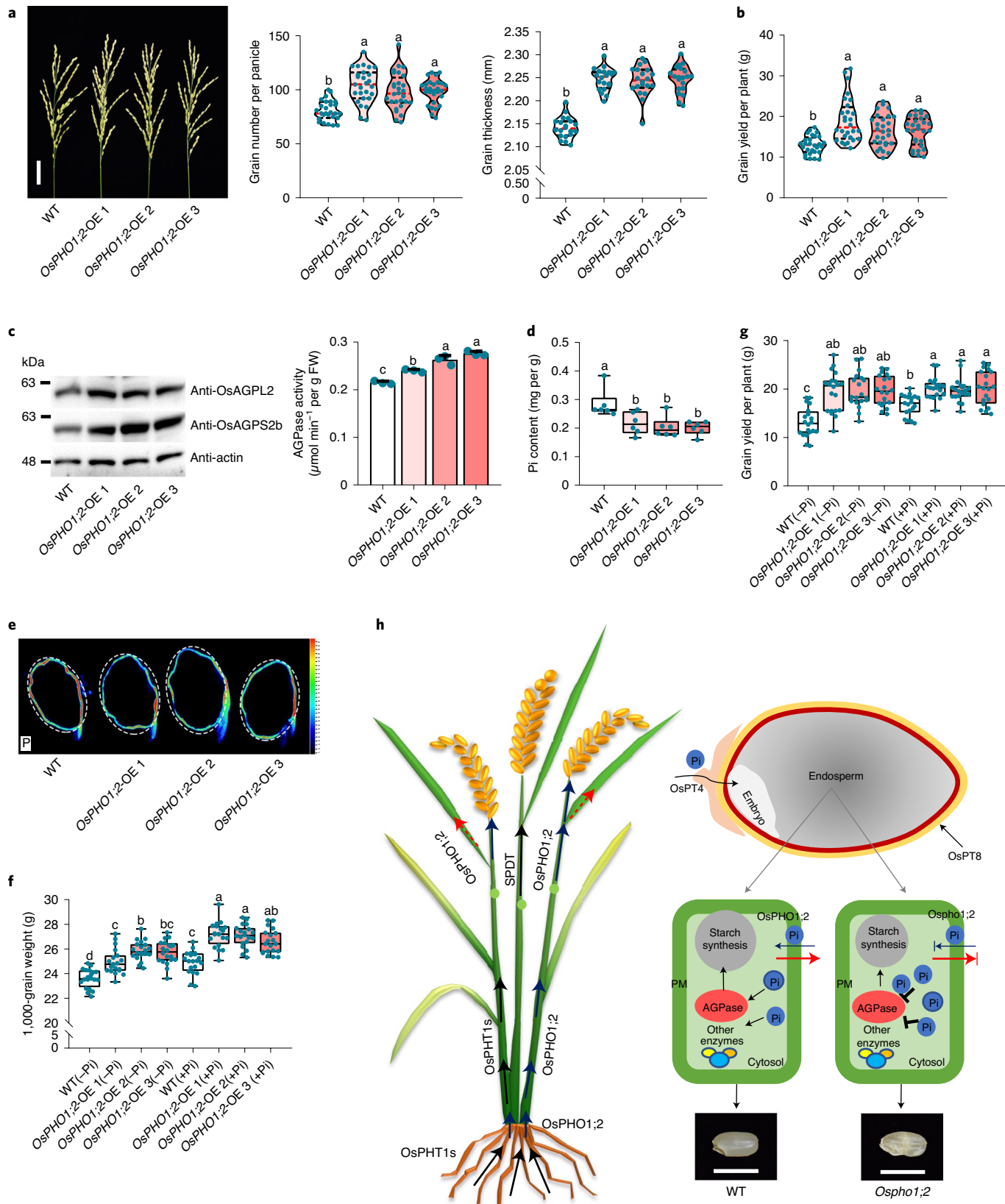
To test whether ectopic overexpression of *OsPHO1;2* improves PUE in the field, we grew overexpressing transgenic lines together with the WT control in the paddy field under P-sufficient and P-deficient conditions (Methods). Major agronomic traits were compared among different lines at harvest. As shown in Fig. 6f,g, 1,000-grain weight and yield increased under both Pi conditions in *OsPHO1;2-OE* lines. This difference was particularly impressive under Pi-deficient conditions, under which *OsPHO1;2-OE* lines scored a 49% yield increase as compared to the WT. Other agronomic traits showed no obvious difference in *OsPHO1;2-OE* lines compared with the WT, except for grain thickness and weight (Supplementary Fig. 9a-d). More importantly, the yield of

Fig. 6 | Ectopic overexpression of *OsPHO1;2* improves grain yield and PUE in transgenic rice. **a,b**, Ectopic overexpression of *OsPHO1;2* significantly increases agronomic values, including panicle size, grain number per panicle and grain thickness (**a**), and grain yield per plant (**b**). Scale bars, 5 cm. $n=24$ plants; red lines, median values; black lines, IQRs in violin plots. **c**, Increased AGPase protein levels and activity in *OsPHO1;2-OE* lines at the grain-filling stage. Values are mean \pm s.d. ($n=3$ independent samples). **d**, Pi content in brown rice of *OsPHO1;2-OE* lines and the WT control at the mature stage ($n=6$ plants). **e**, Total P distribution in WT and *OsPHO1;2-OE* lines in brown rice imaged by the μ XRF spectrometer. Normalized X-ray fluorescence intensities are scaled from red (maximum) to blue (minimum). The actual seed area of each sample is marked by a white dashed line. **f,g**, Comparison of 1,000-grain weight (**f**) and grain yield per plant (**g**) between WT and *OsPHO1;2-OE* lines under conditions of normal (+Pi) and no (-Pi) P-fertilizer utilization in the paddy field ($n=20$ plants). For box-and-whisker plots, the central line, box and whiskers indicate the median, IQR and 1.5 times the IQR, respectively (**d,f,g**). $P=3.48 \times 10^{-8}$ (**a**, middle), $P=4.33 \times 10^{-22}$ (**a**, right), $P=2.10 \times 10^{-6}$ (**b**), $P=6.96 \times 10^{-6}$ (**c**), $P=3.58 \times 10^{-3}$ (**d**), $P=9.02 \times 10^{-29}$ (**f**), $P=6.27 \times 10^{-13}$ (**g**) by one-way ANOVA. Different letters denote significant differences ($P < 0.05$) from Tukey's HSD test (**a-d,f,g**). **h**, A proposed model for *OsPHO1;2* function in facilitating grain filling and Pi reallocation. *OsPHO1;2*, together with *OsPHT1* proteins (*OsPHT1s*), coordinate Pi transportation from roots to above-ground tissues. *OsPT4*, *OsPT8* and *SPDT* are mainly responsible for Pi transportation into seeds. The plasma membrane (PM)-localized *OsPHO1;2* exports excess Pi from the developing endosperm as a major action to maintain Pi homeostasis for proper starch synthesis during grain filling. In *OspHO1;2* mutants, Pi accumulates in endosperm cells, which represses AGPase and other starch-synthesis enzymes, finally resulting in grain-filling defects. Scale bars, 5 mm.

OsPHO1;2-OE lines showed no obvious difference under diverse Pi conditions (Fig. 6g). We therefore conclude that ectopic overexpression of *OsPHO1;2* can improve PUE and grain yield under low-Pi conditions, which will be a useful trait for sustainable production of cereal crops.

Discussion

Pi homeostasis is critical for plant growth and development and should be orchestrated by a large number of Pi transporters^{10,33}. Although developing seeds are a major Pi sink, little is known about how Pi is transported into and out of this important storage tissue.



Our current study reveals the function of a PHO1-type transporter, OsPHO1;2, in Pi reallocation from the developing endosperm, and a similar function is also shared by ZmPHO1;2 in maize. This Pi transporter serves as a Pi-unloading pathway from seeds. It is particularly interesting to find that OsPHO1;2 affects the process of grain filling. In contrast to the *gif1* mutant that fails to unload sucrose into seeds³, the *Ospho1;2* mutant accumulated more soluble sugars in seeds and therefore impacted a downstream process of GIF1 invertase, namely starch synthesis. This notion is supported by the finding of overall downregulation of starch-synthesis enzymes in the mutant. In particular, AGPase acts as a possible target for OsPHO1;2 function, as lack of AGPase causes similar defects as observed in the *Ospho1;2* mutant^{30,31}. Particularly relevant is the allosteric inhibition of AGPase by elevated Pi levels^{5,34}. In addition, Pi levels also appeared to affect *AGPase* gene expression. An earlier study showed that Pi levels were correlated with mRNA levels of *AgpS2* in tobacco, with high Pi levels inhibiting *AgpS2* expression³². Pi over-accumulation in mutant seeds likely triggers a decrease in total enzyme activity of AGPase through suppression of *AGPase* mRNA and allosteric inhibition of the enzyme activity, leading to defects in starch synthesis and grain filling. In support of this conclusion, ectopic overexpression of either one of the two cytosolic AGPases partially restored the grain weight of the *Ospho1;2-ko1* mutant.

As a regulatory factor for the expression and activity of starch-synthesis enzymes, Pi homeostasis must be fine tuned by balancing influx and efflux processes in filling grains. On one hand, Pi, G-1-P and other Pi-containing compounds need to be loaded into developing seeds to support starch synthesis. On the other hand, large amount of free Pi is released as a result of PPi hydrolysis from AGPase activity. Therefore, excess free Pi must be reallocated to maintain homeostasis in endosperm cells and prevent AGPase inhibition in the filling grain. In this context, our study identified OsPHO1;2 as a major Pi transporter that plays an essential role in Pi reallocation and homeostasis in the endosperm. Together with previous studies on other transporters, we propose a model for OsPHO1;2-mediated Pi homeostasis during grain filling (Fig. 6h). Briefly, OsPHT1 proteins are key transporters responsible for Pi uptake and root-to-shoot translocation after OsPHO1;2-mediated loading to xylem, followed by sequential Pi transfer by OsPHO1;2 and OsPHT1 proteins to leaves and panicles through nodes. From there, OsPT4, OsPT8 and SPDT are involved in Pi distribution to developing seeds. In seeds, OsPHO1;2 is important for Pi transportation across the boundary between maternal and filial tissues, similar to the process involving PHO1 in *Arabidopsis* seeds³⁵.

We conclude that OsPHO1;2 likely plays dual roles in Pi homeostasis in the seed, namely unloading Pi from the pericarp into endosperm cells (as a minor action) and exporting excess Pi from the developing endosperm (as a major action) to balance Pi levels in endosperm cells during grain filling, thus fine tuning Pi homeostasis during grain development. In this manner, the Pi level is strictly adjusted by OsPHO1;2 for proper starch synthesis in seeds. This model is also supported by the analysis of *OsPHO1;2*-overexpression lines in which both total P and free Pi levels were significantly reduced in the endosperm. Based on this model, further investigation should resolve mechanistic processes about how various Pi transporters work together to precisely control Pi fluxes across different maternal tissues and endosperm in developing seeds and between sink and source organs. Moreover, this PHO1-type Pi transporter can increase yield (through enhanced grain filling) and improve PUE in cereal crops, providing a promising target gene for breeding crops with high yield under low-P availability in agriculture, which has been a long-term goal in crop breeding.

Online content

Any methods, additional references, Nature Research reporting summaries, source data, extended data, supplementary information,

acknowledgements, peer review information; details of author contributions and competing interests; and statements of data and code availability are available at <https://doi.org/10.1038/s41588-021-00855-6>.

Received: 20 April 2020; Accepted: 24 March 2021;

Published online: 29 April 2021

References

- Yang, J. & Zhang, J. Grain filling of cereals under soil drying. *New Phytol.* **169**, 223–236 (2006).
- Wang, L., Lu, Q., Wen, X. & Lu, C. Enhanced sucrose loading improves rice yield by increasing grain size. *Plant Physiol.* **169**, 2848–2862 (2015).
- Wang, E. et al. Control of rice grain-filling and yield by a gene with a potential signature of domestication. *Nat. Genet.* **40**, 1370–1374 (2008).
- Sosso, D. et al. Seed filling in domesticated maize and rice depends on SWEET-mediated hexose transport. *Nat. Genet.* **47**, 1489–1493 (2015).
- Tuncel, A. & Okita, T. W. Improving starch yield in cereals by over-expression of ADP-glucose pyrophosphorylase: expectations and unanticipated outcomes. *Plant Sci.* **211**, 52–60 (2013).
- Jeon, J. S., Ryoo, N., Hahn, T. R., Walia, H. & Nakamura, Y. Starch biosynthesis in cereal endosperm. *Plant Physiol. Biochem.* **48**, 383–392 (2010).
- Ballicora, M. A., Iglesias, A. A. & Preiss, J. ADP-glucose pyrophosphorylase: a regulatory enzyme for plant starch synthesis. *Photosynth. Res.* **79**, 1–24 (2004).
- Yoshida, K. T., Wada, T., Koyama, H., Mizobuchi-Fukuoka, R. & Naito, S. Temporal and spatial patterns of accumulation of the transcript of myo-inositol-1-phosphate synthase and phytin-containing particles during seed development in rice. *Plant Physiol.* **119**, 65–72 (1999).
- Tagashira, Y., Shimizu, T., Miyamoto, M., Nishida, S. & Yoshida, K. T. Overexpression of a gene involved in phytic acid biosynthesis substantially increases phytic acid and total phosphorus in rice seeds. *Plants* **4**, 196–208 (2015).
- Kopriva, S. & Chu, C. Are we ready to improve phosphorus homeostasis in rice? *J. Exp. Bot.* **69**, 3515–3522 (2018).
- Gu, M., Chen, A., Sun, S. & Xu, G. Complex regulation of plant phosphate transporters and the gap between molecular mechanisms and practical application: what is missing? *Mol. Plant* **9**, 396–416 (2016).
- Zhang, F. et al. Involvement of OsPht1;4 in phosphate acquisition and mobilization facilitates embryo development in rice. *Plant J.* **82**, 556–569 (2015).
- Ai, P. et al. Two rice phosphate transporters, OsPht1;2 and OsPht1;6, have different functions and kinetic properties in uptake and translocation. *Plant J.* **57**, 798–809 (2009).
- Wang, X. et al. Phosphate transporters OsPHT1;9 and OsPHT1;10 are involved in phosphate uptake in rice. *Plant Cell Environ.* **37**, 1159–1170 (2014).
- Chang, M. X. et al. OsPHT1;3 mediates uptake, translocation, and remobilization of phosphate under extremely low phosphate regimes. *Plant Physiol.* **179**, 656–670 (2019).
- Jia, H. et al. The phosphate transporter gene *OsPht1;8* is involved in phosphate homeostasis in rice. *Plant Physiol.* **156**, 1164–1175 (2011).
- Sun, S. et al. A constitutive expressed phosphate transporter, OsPht1;1, modulates phosphate uptake and translocation in phosphate-replete rice. *Plant Physiol.* **159**, 1571–1581 (2012).
- Stefanovic, A. et al. Members of the *PHO1* gene family show limited functional redundancy in phosphate transfer to the shoot, and are regulated by phosphate deficiency via distinct pathways. *Plant J.* **50**, 982–994 (2007).
- Mlodzinska, E. & Zboinska, M. Phosphate uptake and allocation—a closer look at *Arabidopsis thaliana* L. and *Oryza sativa* L. *Front Plant Sci.* **7**, 1198 (2016).
- Secco, D., Baumann, A. & Poirier, Y. Characterization of the rice *PHO1* gene family reveals a key role for OsPHO1;2 in phosphate homeostasis and the evolution of a distinct clade in dicotyledons. *Plant Physiol.* **152**, 1693–1704 (2010).
- Zhao, H. et al. Disruption of *OsSULTR3;3* reduces phytate and phosphorus concentrations and alters the metabolite profile in rice grains. *New Phytol.* **211**, 926–939 (2016).
- Yamaji, N. et al. Reducing phosphorus accumulation in rice grains with an impaired transporter in the node. *Nature* **541**, 92–95 (2017).
- Sun, L. et al. Sugar homeostasis mediated by cell wall invertase GRAIN INCOMPLETE FILLING 1 (GIF1) plays a role in pre-existing and induced defence in rice. *Mol. Plant Pathol.* **15**, 161–173 (2014).
- Krishnan, S. & Dayanandan, P. Structural and histochemical studies on grain-filling in the caryopsis of rice (*Oryza sativa* L.). *J. Biosci.* **28**, 455–469 (2003).
- Kim, H. K. & Lee, S. J. Synchrotron X-ray imaging for nondestructive monitoring of sap flow dynamics through xylem vessel elements in rice leaves. *New Phytol.* **188**, 1085–1098 (2010).

26. Zhang, J. et al. Knockdown of rice microRNA166 confers drought resistance by causing leaf rolling and altering stem xylem development. *Plant Physiol.* **176**, 2082–2094 (2018).
27. Wykoff, D. D. & O'Shea, E. K. Phosphate transport and sensing in *Saccharomyces cerevisiae*. *Genetics* **159**, 1491–1499 (2001).
28. Arpat, A. B. et al. Functional expression of PHO1 to the Golgi and trans-Golgi network and its role in export of inorganic phosphate. *Plant J.* **71**, 479–491 (2012).
29. Tian, Z. et al. Allelic diversities in rice starch biosynthesis lead to a diverse array of rice eating and cooking qualities. *Proc. Natl Acad. Sci. USA* **106**, 21760–21765 (2009).
30. Lee, S. K. et al. Identification of the ADP-glucose pyrophosphorylase isoforms essential for starch synthesis in the leaf and seed endosperm of rice (*Oryza sativa* L.). *Plant Mol. Biol.* **65**, 531–546 (2007).
31. Preiss, J. Regulation of the biosynthesis and degradation of starch. *Ann. Rev. Plant Physiol.* **33**, 431–454 (1982).
32. Nielsen, T. H., Krapp, A., Roper-Schwarz, U. & Stitt, M. The sugar-mediated regulation of genes encoding the small subunit of Rubisco and the regulatory subunit of ADP glucose pyrophosphorylase is modified by phosphate and nitrogen. *Plant Cell Environ.* **21**, 443–454 (1998).
33. Wang, D., Lv, S., Jiang, P. & Li, Y. Roles, regulation, and agricultural application of plant phosphate transporters. *Front Plant Sci.* **8**, 817 (2017).
34. Tuncel, A. et al. The rice endosperm ADP-glucose pyrophosphorylase large subunit is essential for optimal catalysis and allosteric regulation of the heterotetrameric enzyme. *Plant Cell Physiol.* **55**, 1169–1183 (2014).
35. Vogiatzaki, E., Baroux, C., Jung, J. Y. & Poirier, Y. PHO1 exports phosphate from the chalazal seed coat to the embryo in developing *Arabidopsis* seeds. *Curr. Biol.* **27**, 2893–2900 (2017).

Publisher's note Springer Nature remains neutral with regard to jurisdictional claims in published maps and institutional affiliations.

© The Author(s), under exclusive licence to Springer Nature America, Inc. 2021

Methods

Map-based cloning and rice and maize transformation. NIP (*Oryza sativa* subspecies *japonica*) was used as the WT control and transgenic parent. The spontaneous mutant *Osho1;2* (*japonica*) was found in our germplasm collection. For preliminary mapping, the mutant was crossed with ZS97 (*indica*) to generate an *F*₂ segregating population. The mutant plants were successively backcrossed with NIP five times to generate a pair of NILs, namely NIL-*OsPHO1;2* and NIL-*Osho1;2*. The *F*₂ population from the cross of NIL-*OsPHO1;2* and NIL-*Osho1;2* was used for fine mapping of *Osho1;2*. All materials were grown in the Shanghai and Hainan experimental stations. Primers used for mapping are listed in Supplementary Table 1.

For rice transformation, various expression constructs were generated and introduced into the calli generated from mature seed embryos of NIP or mutants through *Agrobacterium* (EHA105)-mediated transformation. For maize transformation, CRISPR-Cas9 (Bar^r) constructs were introduced into immature embryos of the WT inbred line C01 by *Agrobacterium*-mediated transformation. Each transgene generated at least 15 independent transgenic lines (*T*₀), which were grown in the greenhouse or the authorized stations in Shanghai and Hainan, and plants with each maize CRISPR-Cas9 transgene were selfed three times. Homozygous progenies (*T*₁ to *T*₃) were analyzed. All plasmid constructs are listed in Supplementary Table 1. Rice suspension cell lines were developed from calli and routinely maintained in liquid MS medium in an incubator shaker.

Agronomic trait analysis. Seedlings were water incubated in growth chambers with a 14–10-h and 28–22 °C (day–night) cycle for seedling phenotyping. For field experiments, 1-month-old seedlings were transplanted into the paddy yield, and agronomic traits including plant height, seed setting rate, tiller number, grain number per panicle, grain weight per plant, 1,000-grain weight, etc., were analyzed at the mature stage. Grain-filling progress from 0 to 30 DAF was recorded. For disease resistance, 2-month-old plants were inoculated with the leaf bacterial blight pathogen *Xanthomonas oryzae* pv. *oryzae*, and disease resistance was recorded as previously described²⁵.

RNA preparation and sequencing. Total RNA from middle-filling stage seeds from NILs was extracted using the RNeasy Plant Mini kit (74904, Qiagen) and RNA integrity was assessed to determine a RIN number with an Agilent Bioanalyzer 2100 (Agilent Technologies). Qualified total RNA was further purified with the RNA Clean XP kit (A63987, Beckman Coulter) and the RNase-Free DNase Set (79254, Qiagen). The quality of RNA samples was assessed by the NanoDrop ND-2000 and the Agilent Bioanalyzer 2100. Next, RNA-seq was performed by the Shanghai Biotechnology Corporation.

qPCR and western blot analysis. Total RNA was prepared from various rice tissues (root, young leaf, elongating stem and node, sheath, inflorescence meristem, young panicle, spikelet and developing seed) using TRIzol reagent methods. For generation of transcripts, 1 µg total RNA was used for cDNA synthesis with a reverse transcription kit (R123-01, Vazyme). For qRT-PCR analysis, a 20-µl volume was used with 2 µl cDNA, 0.5 µM specific primers and 10 µl 2× SYBR Green Mix (RR420A, Takara), supplemented to 20 µl with ddH₂O, on a Bio-Rad real-time PCR machine according to the manufacturer's instructions. The rice *Actin* gene was used as the internal control. All primers used for qRT-PCR analysis are listed in Supplementary Table 1.

For western blotting, total proteins were extracted with extraction buffer consisting of 50 mM Tris-HCl (pH 8.0), 0.25 M sucrose, 2 mM dithiothreitol, 2 mM EDTA and 1 mM phenylmethylsulfonyl fluoride. Proteins were resolved by SDS-PAGE (GSG2001-10T, EZBiolab) and then transferred to a PVDF membrane. The membrane was then incubated with primary and secondary antibodies and visualized using ECL Plus reagent. To develop the OsPHO1;2-specific antibody, the C-AGQQPSASEDEE peptide was chemically synthesized and used as antigen injected into a rabbit to yield serum (1:500, Abmart). Antibodies specific to OsAGPL2 and OsAGPS2b³⁶ (1:1,500, Abmart) were provided by the J. Wan laboratory (Nanjing Agricultural University), and the antibody specific to Bt2 (ADP-Glc pyrophosphorylase in maize, AS111739) was purchased from Agrisera (Supplementary Table 3).

Subcellular localization analysis. Rice sheath protoplasts were used to perform subcellular localization analysis. For expression plasmid constructs, full-length CDSs were generated by PCR and cloned into pA7-YFP/eGFP/mCherry. Constructs and primers used are listed in Supplementary Tables 1 and 2. Plasmids (10 µg) were transformed into rice protoplasts, and fluorescence images were recorded using a Zeiss LSM 880 or an Olympus FV1000 confocal laser microscope.

For transient expression analysis in onion cells, the particle bombardment method was performed. In brief, 3 µg plasmid in a 10-µl volume was mixed with 10 µl 60 mg ml⁻¹ gold particle solution, 10 µl 2.5 M CaCl₂ and 4 µl 0.1 M spermidine. Gold particles were bombarded into onion cells. Bombarded onion cells were grown on MS medium at 30 °C overnight. Fluorescence images were recorded with an Olympus confocal laser microscope.

For immunogold labeling analysis, node I and developing seed tissues from NIP were used to detect immunogold labeling signals according to a method

described previously³⁷ with little changes. In detail, sections were fixed in 4% (wt/vol) paraformaldehyde and 0.5% (vol/vol) glutaraldehyde in 0.05 M PIPES, pH 7.0, and stored at 4 °C overnight. Next, sections were washed with 0.05 M PIPES three times, followed by fixing in 2% (wt/vol) osmium tetroxide in 0.05 M PIPES for 1 h at room temperature. Sections were dehydrated through a graded ethanol series and slowly embedded in LR White resin for several days. Ultrathin sectioning was performed using a Leica Ultracut R microtome with a diamond knife, and 60–80-nm-thick sections were collected on nickel grids. For immunolabeling, nickel grids carrying ultrathin sections were first exposed to 10% H₂O₂ for 10 min and then blocked with 1% (wt/vol) BSA in 0.1 M PBS for 1 h at room temperature. Nickel grid sections were then incubated with the anti-OsPHO1;2 antibody (diluted 1:20 with 1% (wt/vol) BSA in 0.1 M PBS) or 1% BSA (negative control) at 4 °C overnight. After washing three times with 0.05% Tween-20 in PBS, nickel grids were transferred and incubated with anti-rabbit IgG (whole-molecule 10-nm colloidal gold particles)-gold antibody (Sigma, G7402) (diluted 1:30) at 37 °C for 2 h. After washing at least six times with PBST and distilled water, grids were stained with 2% (wt/vol) aqueous uranyl acetate for 5 min and lead citrate for 3 min. Finally, grids were examined with a transmission electron microscope (H7650, Hitachi) using a voltage of 80 kV.

Tissue-specific expression of OsPHO1;2. For GUS histochemical staining analysis, the 3-kb promoter sequence of *OsPHO1;2* was cloned into the pCambia-1300 vector to generate the GUS fusion reporter *pOsPHO1;2-GUS* (Supplementary Table 2) that was introduced into NIP plants. Plant tissues obtained from *pOsPHO1;2-GUS*-transgenic plants were stained with GUS staining solution (100 mM sodium Pi buffer, pH 7.0, 10 mM EDTA, 1 mM X-gluc and 0.1% (vol/vol) Triton X-100) as usual.

For immunofluorescence assays, immunostaining was performed using tissues from node I and early-filling stage seeds of WT rice as described previously³⁸ with slight modifications. In brief, tissues were fixed in 4% (wt/vol) paraformaldehyde and 60 mM Suc buffered with 50 mM cacodylic acid (pH 7.4) for 2 h at room temperature. After washing three to four times with 60 mM Suc and 50 mM cacodylic acid (pH 7.4), fixed samples were embedded in 5% agar and sectioned to 100 µm in thickness. Sections were placed on microscope slides, followed by incubation with PBS at 30 °C for 2 h and then reincubated with PBS at 30 °C for 2 h, washed three times with PBS and blocked with 5% (wt/vol) BSA in PBS. Slides were then incubated with purified rabbit anti-OsPHO1;2 polyclonal antibodies (1:100 dilution in PBS) or rabbit anti-GUS polyclonal antibodies (1:500, ab50148, Abcam, Supplementary Table 3) at 24 °C overnight. After five washes with PBS and blocking with 5% (wt/vol) BSA in PBS, slides were incubated with secondary antibodies (goat anti-rabbit IgG, 1:500, A-11010, Thermo Fisher, Supplementary Table 3) for 2 h at 24 °C, washed five times with PBS and covered with 50% (vol/vol) glycerol in PBS. The fluorescence signal was observed with an Olympus FV1000 confocal laser scanning microscope.

AGPase and other starch-synthesis isozyme activity assays. Dehulled seeds (50 mg) during grain filling were ground and resuspended in 500 µl lysis buffer containing 100 mM Tricine-NaOH (pH 8.0), 8 mM MgCl₂, 2 mM EDTA, 50 mM β-mercaptoethanol, 12.5% (vol/vol) glycerol and 5% (wt/vol) PvPP40. After centrifugation at 10,000 r.p.m. (4 °C) for 10 min, supernatants (crude extractions) were collected for the assay. The AGPase activity assay was conducted in 100 mM HEPES-NaOH (pH 7.4), 1.2 mM ADP-Glc, 3 mM pyrophosphate, 5 mM MgCl₂ and 4 mM dithiothreitol at 30 °C, and 50 µl of crude extractions was added with a total reaction volume of 250 µl as previously described³⁹. Twenty minutes later, enzymes were inactivated by placing the mixture in a boiling water bath for 2 min, and samples were mixed with 30 µl NADP (2 mM). Enzymatic activity was recorded as the increase in OD₃₄₀ after the addition of 1 µl each of phosphoglucomutase (0.4 U, Roche) and G6P dehydrogenase (0.35 U, Sigma). For isozyme activity, starch synthase and branching enzyme isozymes were separated by native PAGE and assayed according to the method described by Nishi et al.⁴⁰, and analysis of debranching enzymes was performed as described by Fujita et al.⁴¹.

AGPase expression in *E. coli*. For AGPase expression in *E. coli*, both full-length CDSs of OsAGPL2 and OsAGPS2b were cloned into the vector pET-Duet to generate the construct pET-Duet-OsAGPL2-OsAGPS2b (primers are listed in Supplementary Table 1), which was transformed into Rosetta competent cells. Expression of fusion protein or the empty control was induced by 20% IPTG at 18 °C, with different concentrations of Pi added.

For detection of AGPase activity in *E. coli*, bacterial precipitation after centrifugation was resuspended in extraction buffer (50 mM Tris-HCl, pH 6.8, 5 mM MgCl₂, 5 mM 2-mercaptoethanol, 5.55% glycerol, 1 mM EDTA, 1 mM EGTA and 0.1 mM phenylmethylsulfonyl fluoride). Crude enzymes were obtained by sonication and centrifugation. Enzyme production was determined by immunodetection. Equal amounts of enzyme proteins were loaded for the AGPase assay, using the same method as described above.

Functional complementation in yeast. The full-length CDS of *OsPHO1;2* was cloned into the vector pAG426GPD-ccdB, and constructs were then transformed into the yeast Pi transport-deficient mutant EY917 (ref. ²⁷) (Supplementary Table

4). Transformed yeast was grown in synthetic dropout (Trp^-) selection medium (pH 5.8) overnight, and 5- μl aliquots of each serial dilution were spotted on agar plate medium ($\text{Trp}^- \text{Ura}^+$) supplemented with different Pi concentrations (0–20 mM Pi). Plates were incubated at 30°C for 3 d to observe yeast growth.

Patch-clamping experiments for Pi transporter activity. Full-length CDSs of *OsPHO1;2*, *Ospho1;2*, *OsPHO1;1* and *OsPHO1;3* were cloned into the vector pEGFP-C1 for expression in mammalian HEK293T cells (Supplementary Tables 1 and 2). Plasmids for transfection were extracted from *E. coli* (DH5 α) using the Qiagen Plasmid Mini kit, and 2 μg plasmid in total was added into each well of six-well plates (Nunc). HEK293T cells were cultured in DMEM supplemented with 10% FBS in a 5% CO₂ incubator at 37°C in moist atmosphere. Cultured HEK293T cells were then transfected with plasmids using the Lipofectamine 3000 Transfection Reagent Kit (Invitrogen). After 48 h of growth, HEK293T cells showing bright green fluorescence were used for patch-clamp experiments.

Whole-cell patch-clamp experiments were performed using an Axopatch 200B patch-clamp setup (Axon Instruments) with a Digitata 1550 digitizer (Axon Instruments) as previously reported^{12,43}. pCLAMP 10.7 software (Axon Instruments) was used for data acquisition and analysis. The bath solution for Pi currents contained 150 mM *N*-methyl-D-glucamine (NMDG), 50 mM PO₄³⁻, 10 mM HEPES, pH 7.5 (adjusted with NMDG), and the pipette solution contained 150 mM NMDG, 50 mM PO₄³⁻, 10 mM EGTA, 10 mM HEPES, pH 7.5 (adjusted with NMDG). A step voltage protocol with a duration of 100 ms for each voltage from -180 mV to +100 mV with a +20-mV step was used for current recordings in HEK293T cells for 1 min after accessing a whole-cell configuration.

For two-electrode voltage-clamp recording of *Xenopus* oocytes, full-length CDSs for *OsPHO1;1*, *OsPHO1;2*, *Ospho1;2* and *OsPHO1;3* were cloned into the pGEMHE oocyte expression vector (Supplementary Tables 1 and 2). Capped RNA was synthesized from 1 μg of linearized plasmid DNA template using the mMESSAGE mACHINE T7 kit (Ambion) according to the manufacturer's instructions. First, 10 ng of each capped RNA, in a total volume of 32.2 nL, was injected into each oocyte. Injected oocytes were incubated in ND96 solution (96 mM NaCl, 2 mM KCl, 1 mM MgCl₂, 1.8 mM CaCl₂, 10 mM HEPES-NaOH, pH 7.4) supplemented with 10 mM Pi at 18°C for 2 d before two-electrode voltage-clamp recording. Oocytes were voltage clamped using a TEV-200A amplifier (Dagan) and monitored by computer through the Digidata 1550 A/D converter and pCLAMP 10.2 software (Axon Instruments)⁴⁴. The standard bath solution contained 10 mM (NMDG)-phosphate and 80 mM mannitol, and pH was adjusted with MES or Tris to 5.5, 6.5 or 7.5. Voltage steps were applied from +60 to -180 mV in -20-mV decrements during 100 ms.

Determination of starch and soluble sugar content in mature seeds.

For determination of total starch concentration, 100 mg rice flour from NILs was measured with the starch assay kit Megazyme K-TSTA (Megazyme). For determination of soluble sugar (including sucrose, glucose and fructose) content, 400 mg brown rice was ground thoroughly with liquid nitrogen and then incubated with 1 ml water in a boiling water bath for 20 min, followed by tenfold dilutions, and supernatants were filtered through a 0.45- μm Millipore filter after centrifugation. Samples were analyzed using an ion chromatograph (ICS-3000, Dionex).

Measurement of Pi and total P content. Various tissues from NILs and WT, *Ospho1;2-ko1* and transgenic plants were harvested and dried at 70°C for 3 d and then ground into powder. Each 50-mg sample was resuspended in 1 ml lysis buffer (12.5% (vol/vol) TCA, 25 mM MgCl₂), followed by vortexing overnight at 4°C. The suspension was centrifuged at 10,000 $\times g$ for 10 min at 4°C. Supernatants (500 μl) were collected and diluted five times with double-distilled water, and diluted supernatants were mixed with 5:1 ammonium vanadate molybdate developer (100 g l⁻¹ ammonium molybdate, 2.35 g l⁻¹ ammonium vanadate and 165 mL⁻¹ 65% HNO₃). Absorption values at 400 nm for the solution were recorded using a microplate reader. Pi concentration was calculated from a standard curve generated by varying concentrations of KH₂PO₄.

Total P measurements were conducted as described previously⁴⁵. Brown rice powders (10 mg) were digested with 1 ml 65% HNO₃. Total P levels were measured with an inductively coupled plasma optical emission spectrometer (Optima 8000DV, PerkinElmer).

μ XRF element fluorescence imaging. High-resolution distribution analysis of P in brown rice was analyzed using a μ XRF spectrometer (M4 Tornado, Bruker). Parameters were set as follows according to the manufacturer's instructions: excitation, 50 kV, 600 μA ; vacuum path, silicon drift detector; detector energy resolution <150 eV; and X-ray beam spot size \leq 20 μm for Mo-K. Cross-sections of seeds from NIL-*OsPHO1;2*, NIL-*Ospho1;2*, WT and *Ospho1;2-ko1* plants and ectopic overexpression plants were imaged, and the relative abundance of P was determined according to the fluorescence intensity.

³¹P nuclear magnetic resonance spectroscopy. Seedling roots were used for the experiment according to the protocol in ref.⁴⁶. In brief, 50 mg of 2-week-old seedling roots were packed into an NMR tube with a diameter of 5 mm equipped

with a perfusion system connected to a peristaltic pump. *In vivo* ³¹P NMR spectra of seedling roots were recorded on a Bruker Ascend 600 spectrometer with MestReNova software version 6.1.1-6384. The ³¹P NMR spectra were recorded at 242.9 MHz lock with deuterioxide in the capillary and water. Chemical shifts were measured relative to the signal from a glass capillary containing 10 mM methylenediphosphonic acid (18.9 ppm relative to 85% H₃PO₄).

P-fertilizer field treatment. For P-fertilizer field treatments, 1-month-old seedlings of WT and overexpression lines were transplanted into two protected paddy fields. One field was normally supplied with commercial P fertilizer, and the other field went without P fertilizer during the whole growth season. Both were equally watered and supplied with N and K fertilizers. Upon maturation, yield components were measured and compared.

Ethics. *Xenopus* oocytes were used to detect patch-clamping transporter activities in this study as mentioned above, and all *Xenopus* oocyte experiments were completed in accordance with animal research ethics regulations.

Statistical analysis. In this study, all values are presented as mean \pm s.d. or s.e.m., and numbers (*n*) of samples or replicates are indicated in figure legends. Significance levels of differences were calculated by Student's *t*-test for pairwise comparisons and by one-way ANOVA followed by Tukey's test for multiple-group comparison and are indicated with *P* values or different letters. Data were analyzed with GraphPad Prism 8.0 and Excel 2013 to perform two-tailed Student's *t*-tests and with Minitab 18 software to perform one-way ANOVA followed by Tukey's test for multiple comparisons. pCLAMP 10.7 software (Axon Instruments) was used for data acquisition and analysis of patch-clamp results.

Reporting Summary. Further information on research design is available in the Nature Research Reporting Summary linked to this article.

Data availability

Entire RNA-seq datasets were deposited in the NCBI Gene Expression Omnibus under accession number GSE149101. Source data are provided with this paper.

References

36. Tang, X. J. et al. ADP-glucose pyrophosphorylase large subunit 2 is essential for storage substance accumulation and subunit interactions in rice endosperm. *Plant Sci.* **249**, 70–83 (2016).
37. Chen, J. H. et al. Nuclear-encoded synthesis of the D1 subunit of photosystem II increases photosynthetic efficiency and crop yield. *Nat. Plants* **6**, 570–580 (2020).
38. Yamaji, N. & Ma, J. F. Spatial distribution and temporal variation of the rice silicon transporter Lsi1. *Plant Physiol.* **143**, 1306–1313 (2007).
39. Nakamura, Y., Yuki, K., Park, S. Y. & Ohya, T. Carbohydrate metabolism in the developing endosperm of rice grains. *Plant Cell Physiol.* **30**, 833–839 (1989).
40. Nishi, A., Nakamura, Y., Tanaka, N. & Satoh, H. Biochemical and genetic analysis of the effects of amylose-extender mutation in rice endosperm. *Plant Physiol.* **127**, 459–472 (2001).
41. Fujita, N. et al. Purification, characterization, and cDNA structure of isoamylase from developing endosperm of rice. *Planta* **208**, 283–293 (1999).
42. Xu, L. et al. Identification of vacuolar phosphate efflux transporters in land plants. *Nat. Plants* **5**, 84–94 (2019).
43. Liu, J. et al. A vacuolar phosphate transporter essential for phosphate homeostasis in *Arabidopsis*. *Proc. Natl Acad. Sci. USA* **112**, E6571–E6578 (2015).
44. Pan, Y. et al. Dynamic interactions of plant CNGC subunits and calmodulins drive oscillatory Ca²⁺ channel activities. *Dev. Cell* **48**, 710–725 (2019).
45. Hansen, T. H. et al. Micro-scaled high-throughput digestion of plant tissue samples for multi-elemental analysis. *Plant Methods* **5**, 12 (2009).
46. Wang, C. et al. Rice SPX-Major Facility Superfamily 3, a vacuolar phosphate efflux transporter, is involved in maintaining phosphate homeostasis in rice. *Plant Physiol.* **169**, 2822–2831 (2015).

Acknowledgements

We thank J. F. Ma for useful discussions, G. Xu for providing the yeast mutant line, expression vector and advice about Pi application, J. Wan for providing OsAGPL2- and OsAGPS2b-specific antibodies, W. Zhang for maize transformation, Q. Shu for rice materials, J. Gong and D. Chao for assistance with P measurements, X. Gao and Z. Zhang for sample preparation and electron microscopic observations. This work was supported by the National Key Research and Development Program of China (2016YFD0100600), the Chinese Academy of Sciences (XDB27040201) and the National Key Laboratory of Plant Molecular Genetics. This work was also supported, in part, by a grant from the National Science Foundation (MCB-1714795 to S.L.) and the National Natural Science Foundation of China (31871217).

Author contributions

Z.H., S.L. and W.T. conceived and designed the research. B.M., L.Z., Q.G., J.W., X.L., H.W., Y.L., J.L., X.W., Q.L. and Y.D. performed experiments. B.M., L.Z., Q.G., J.W. and Z.H. analyzed data and oversaw the entire study. B.M., L.Z., Q.G., W.T., S.L. and Z.H. wrote the manuscript.

Competing interests

The authors declare no competing interests.

Additional information

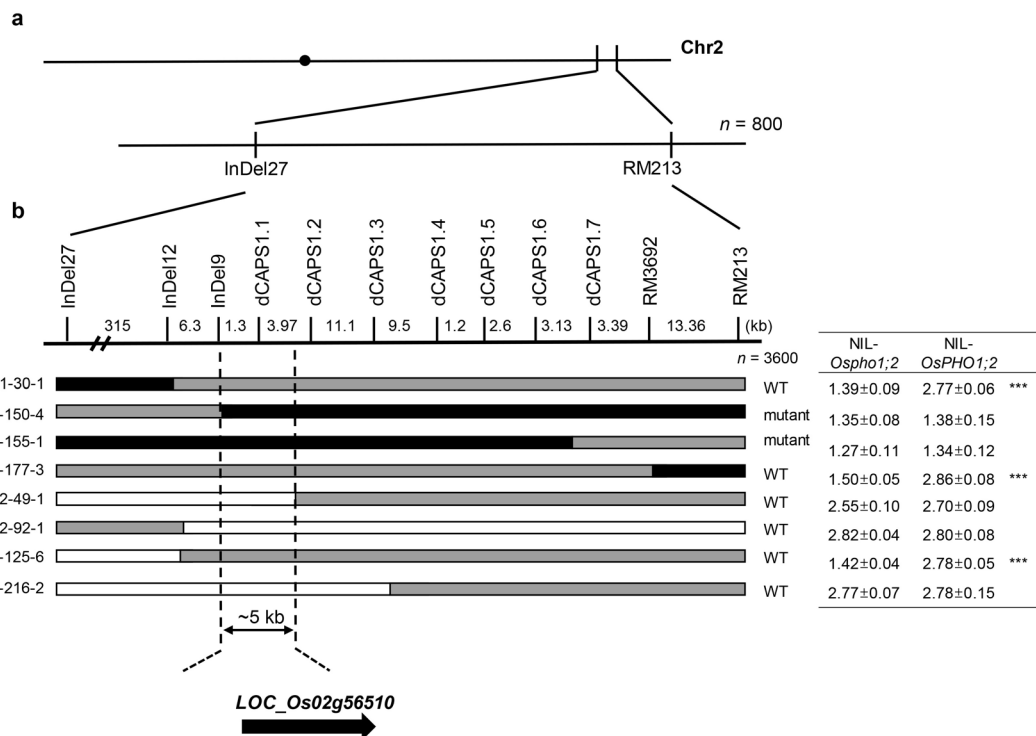
Extended data is available for this paper at <https://doi.org/10.1038/s41588-021-00855-6>.

Supplementary information The online version contains supplementary material available at <https://doi.org/10.1038/s41588-021-00855-6>.

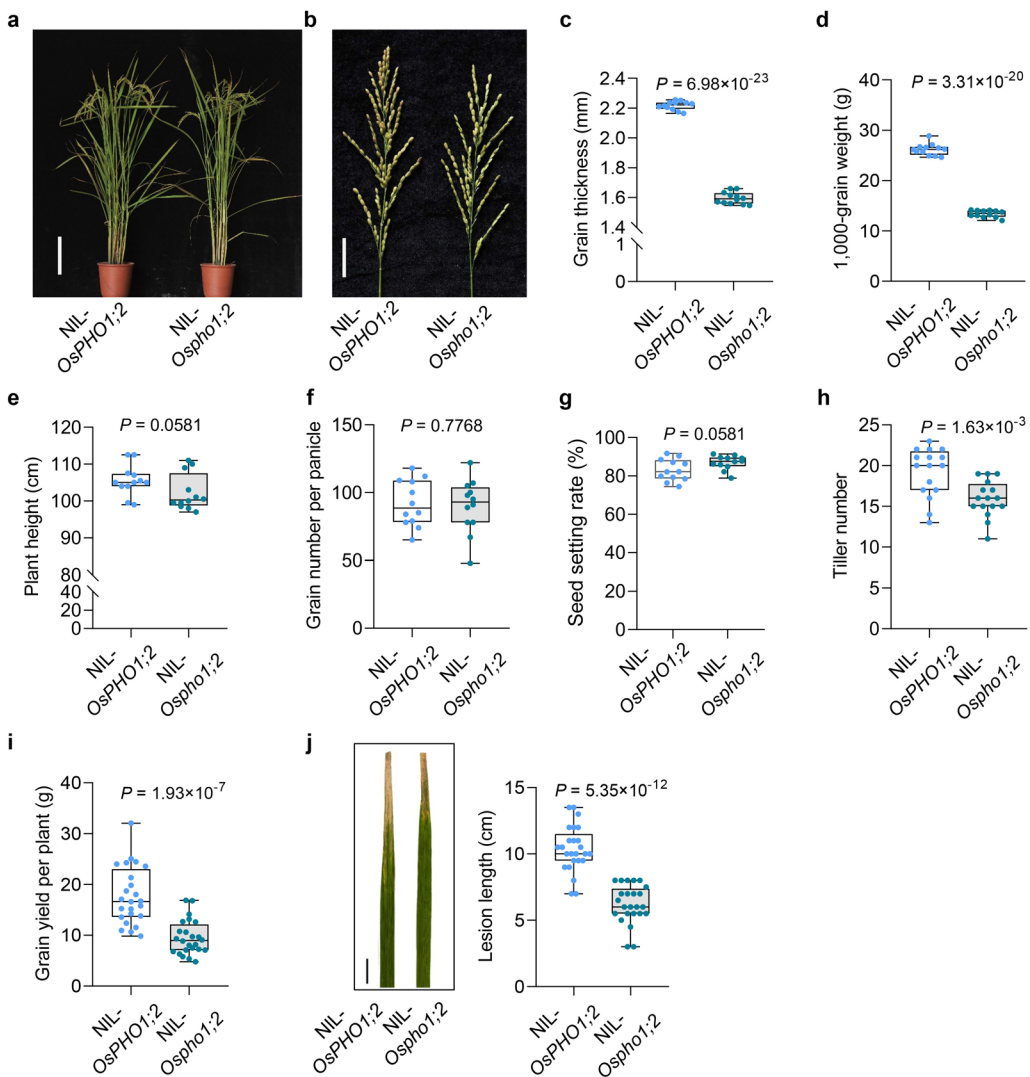
Correspondence and requests for materials should be addressed to W.T., S.L. or Z.H.

Peer review information *Nature Genetics* thanks the anonymous reviewer for their contribution to the peer review of this work.

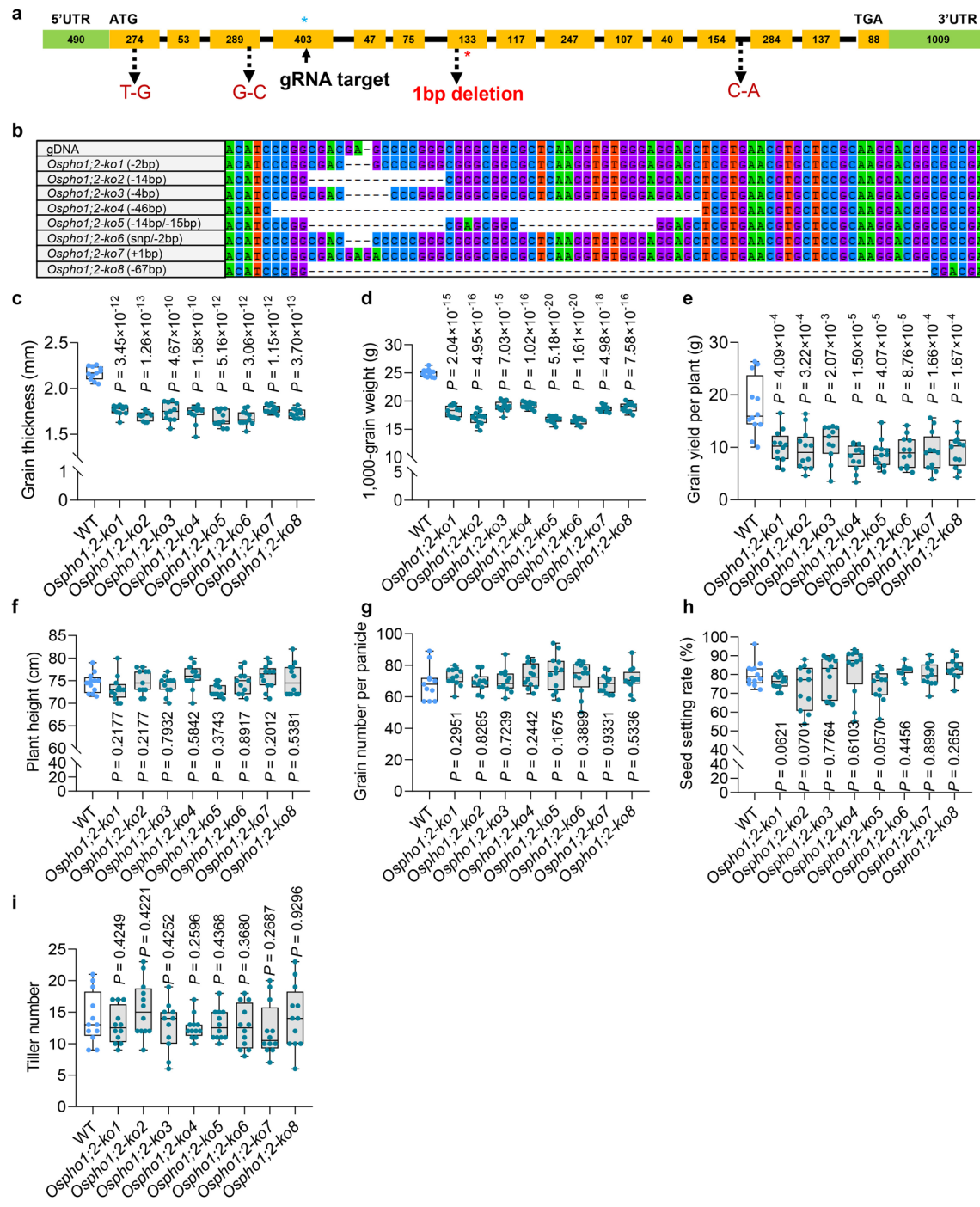
Reprints and permissions information is available at www.nature.com/reprints.



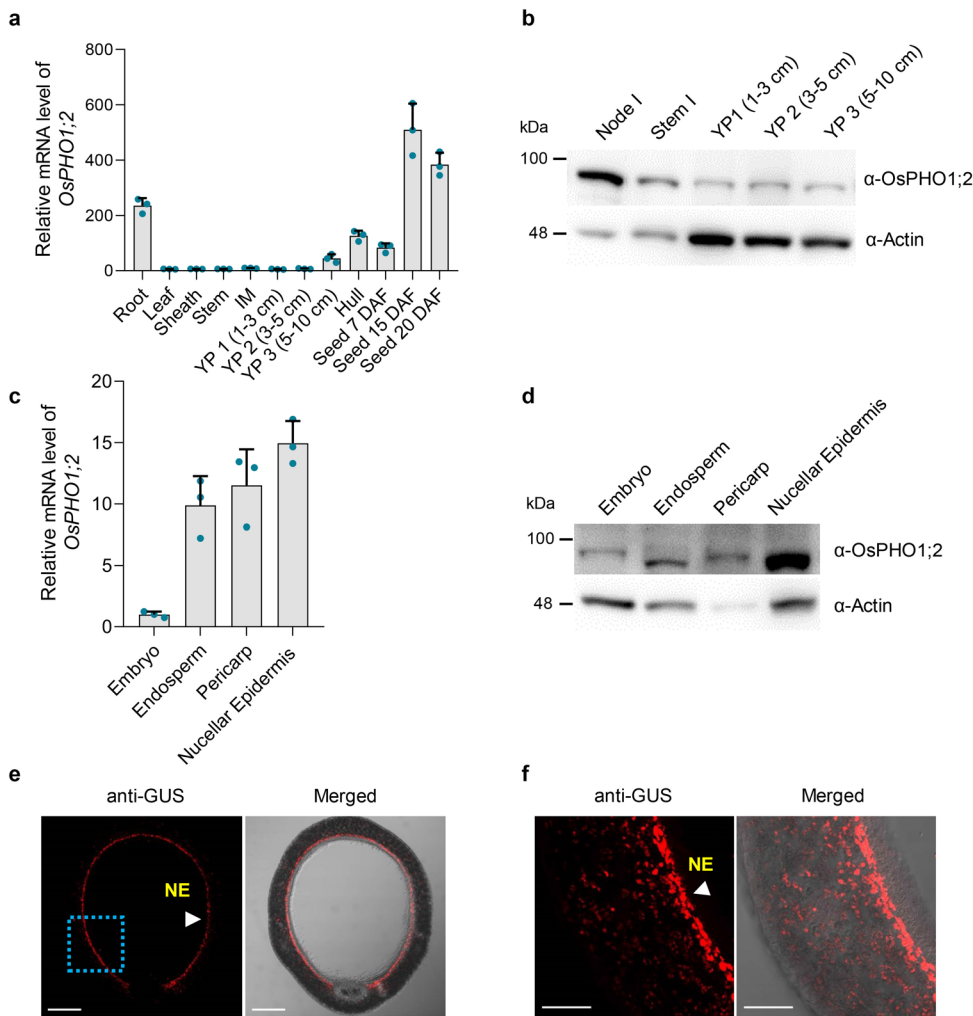
Extended Data Fig. 1 | Map-based cloning of *Ospho1;2* for grain incomplete filling phenotype. Primary mapping region **a** and fine mapping **b** of the locus to a ~5 kb region of the NIP genome with 3600 individuals from NILs population, denoted by double black headed arrowheads. This fine mapping region includes only one gene *LOC_Os02g56510* that encodes OsPHO1;2. Eight recombinants delimiting the mapping region for detailed progeny analysis is presented by bars. Grey bars refer to the heterozygous allele, white and black bars refer to NIL-OsPHO1;2 and NIL-Ospho1;2 homozygous alleles, respectively. Phenotypic statistics of 100-grain weight from F₃ segregation of the 8 recombinants were shown on the right. Data are means ± s.d. (n=8 plants). *** indicates significant difference at P < 0.001 according to two-tailed Student's t-test. 1-30-1: P = 2.88 × 10⁻¹⁵; 1-177-3: P = 7.10 × 10⁻¹⁵; 2-125-6: P = 3.31 × 10⁻¹⁸.



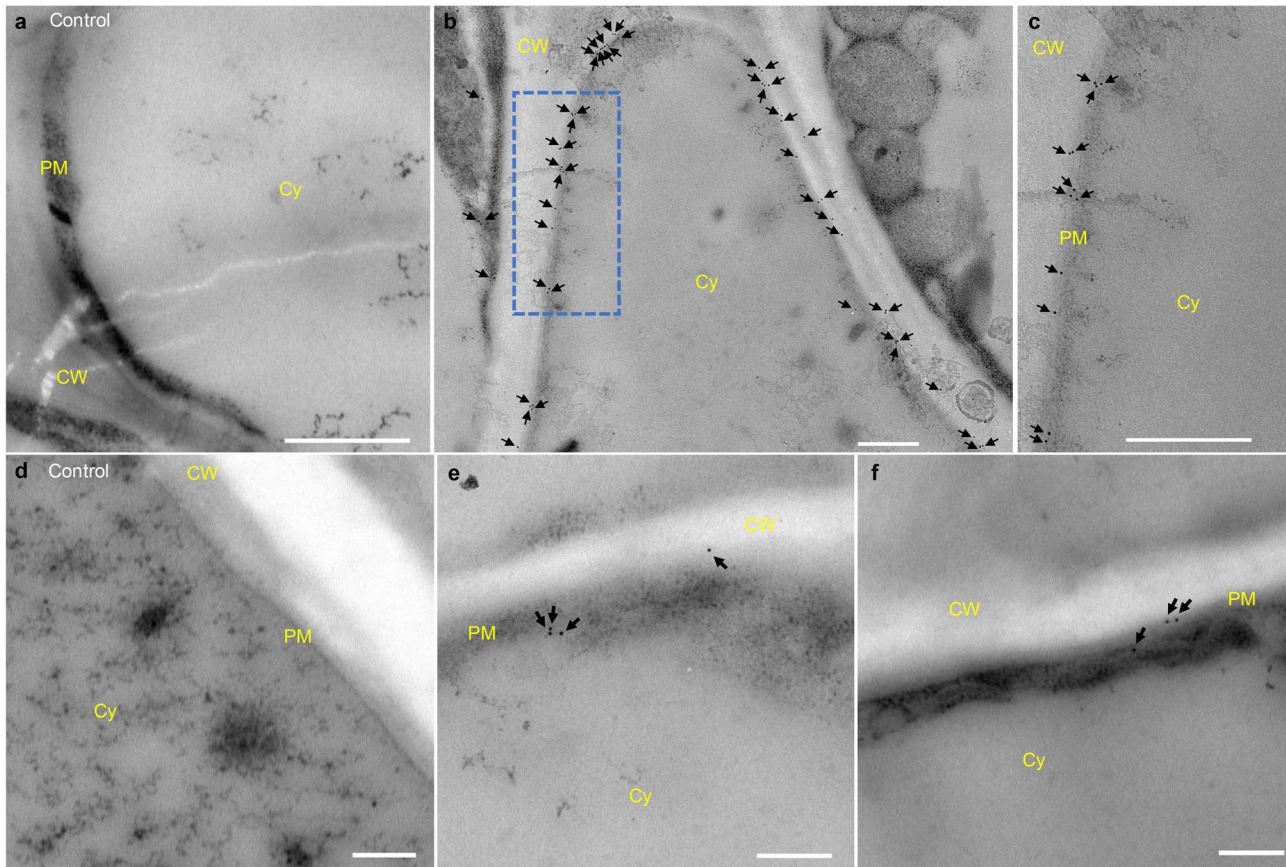
Extended Data Fig. 2 | Agronomic traits of nearly isogenic lines of *OsPHO1;2* and *Ospho1;2*. **(a, b)** Morphology of mature plants **a** and panicles **b** of NIL-*OsPHO1;2* and NIL-*Ospho1;2*. Scale bars, 20 cm **a** and 5 cm **b**, respectively. **(c-i)** Comparison of grain thickness **(c)**, 1,000-grain weight **(d)**, plant height **(e)**, grain number per panicle **(f)**, seed setting rate **(g)**, tiller number **(h)** and grain yield per plant **(i)** between NIL-*OsPHO1;2* and NIL-*Ospho1;2*. **(j)** Lesions and lesion length of the representative NIL plants inoculated with *Xanthomonas oryzae* pv. *oryzae* (*Xoo*) (strain PXO99A) for 2 weeks, indicating that *Ospho1;2* mutant plants significantly increased *Xoo* resistance. Scale bars, 2 cm. $n=12$ plants for **c-g**, $n=16$ plants for **h**, $n=24$ plants for **i** and **j**. P -values were indicated according to two-tailed Student's *t*-test **(c-j)**. For the box-and-whisker plots, the central line, box and whiskers indicate the median, IQR and 1.5 times the IQR, respectively **(c-j)**.



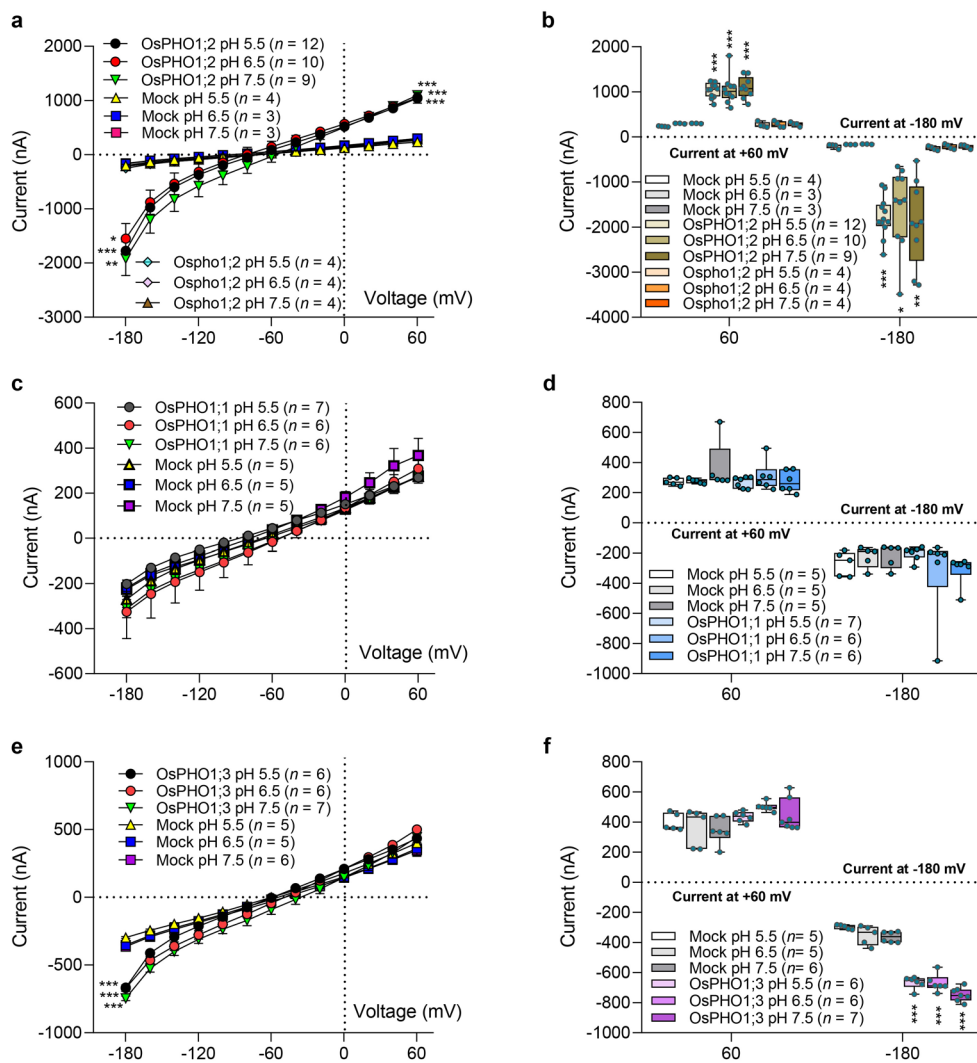
Extended Data Fig. 3 | Mutant sites and agronomic traits of CRISPR-Cas9 knockout alleles. **a**, Gene structure and mutation sites in *OsPHO1;2*, including nucleotide substitutions and deletions. **b**, Different mutant alleles (*Ospho1;2-ko1* to *Ospho1;2-ko8*) generated by CRISPR-Cas9 in Nip background, and the mutant target was indicated in **(a)** with blue star. **(c-i)** Trait comparison of grain thickness **(c)**, 1,000-grain weight **(d)**, grain yield per plant **(e)**, plant height **(f)**, grain number per panicle **(g)**, seed setting rate **(h)** and tiller number **(i)** between wild type and various mutant alleles. $n=12$ plants for **c-j**. P -values were indicated according to two-tailed Student's *t*-test. For the box-and-whisker plots, the central line, box and whiskers indicate the median, IQR and 1.5 times the IQR, respectively **(c-i)**.



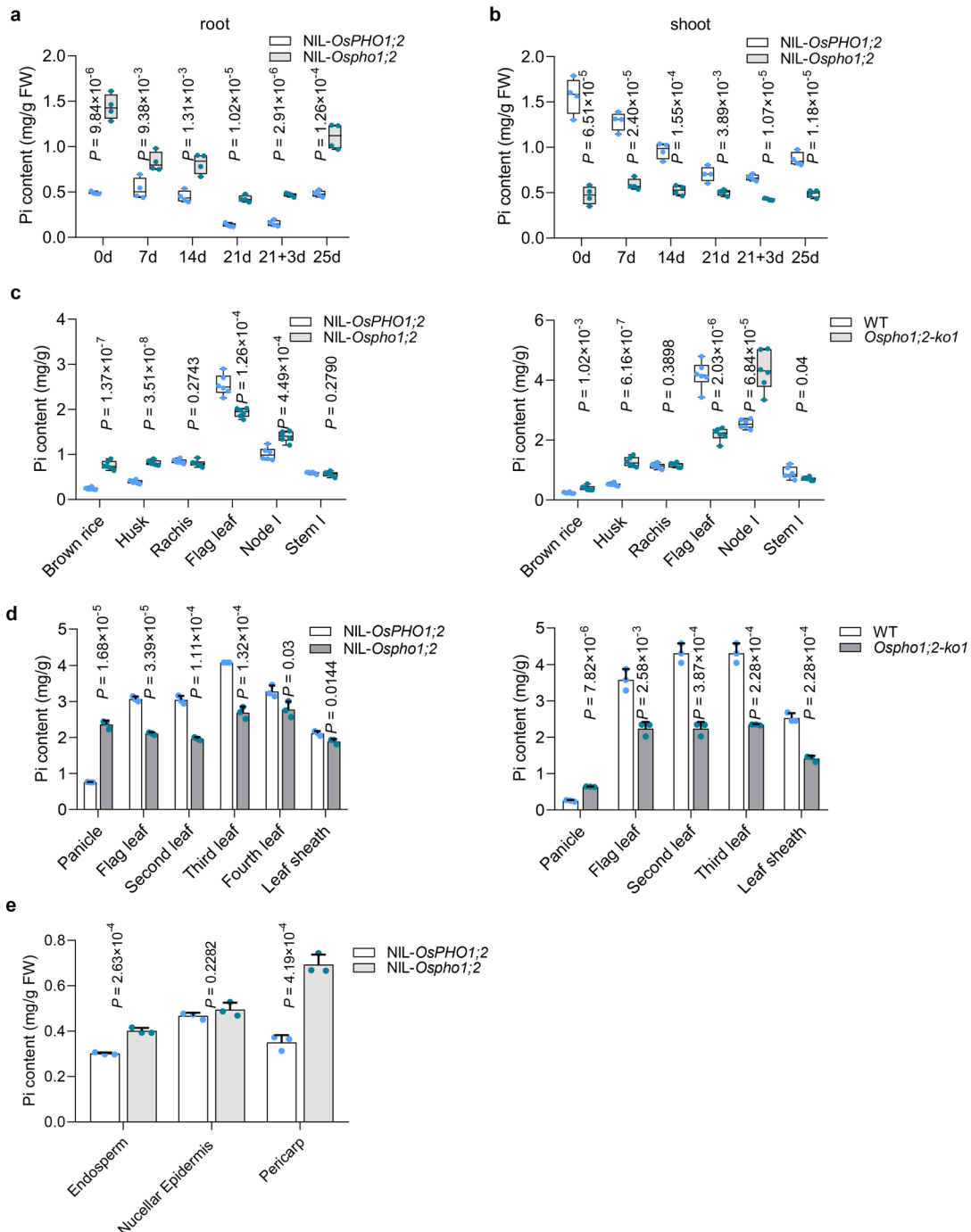
Extended Data Fig. 4 | Tissue specific expression pattern of *OsPHO1;2*. **a**, mRNA levels of *OsPHO1;2* in different tissues by qRT-PCR, normalized to the rice *Actin* gene. IM, inflorescence meristem; YP, young panicle; hull, and filling seeds. Values are means \pm s.d. ($n=3$ technical replicates). **b**, Western blot detection of *OsPHO1;2* in various tissues using anti-*OsPHO1;2*, and Actin was immunodetected as a loading control. **c**, qRT-PCR analysis of relative mRNA levels of *OsPHO1;2* in different developing seed tissues, including embryo, endosperm, pericarp and nucellar epidermis, normalized to the rice *Actin* gene. Data are means \pm s.d. ($n=3$ technical replicates). **d**, Western blot analysis of *OsPHO1;2* in developing seed tissues using anti-*OsPHO1;2*, and anti-*Actin* was immunodetected as a loading control. **e**, Tissue specificity of *OsPHO1;2* expression in early-milking seeds. Immunostaining with an anti-GUS antibody was performed in milky grains (5 DAF) of transgenic lines with *pOsPHO1;2-GUS* fusion reporter driven by the native promoter. The image is a representative of three independent lines. Scale bars, 200 μ m. **f**, Blue box area in (c) was magnified. Scale bars, 50 μ m. The white arrowheads indicate the nucellar epidermis (NE, e, f). Independent experiments were repeated at least 2 times with similar results (a-f).



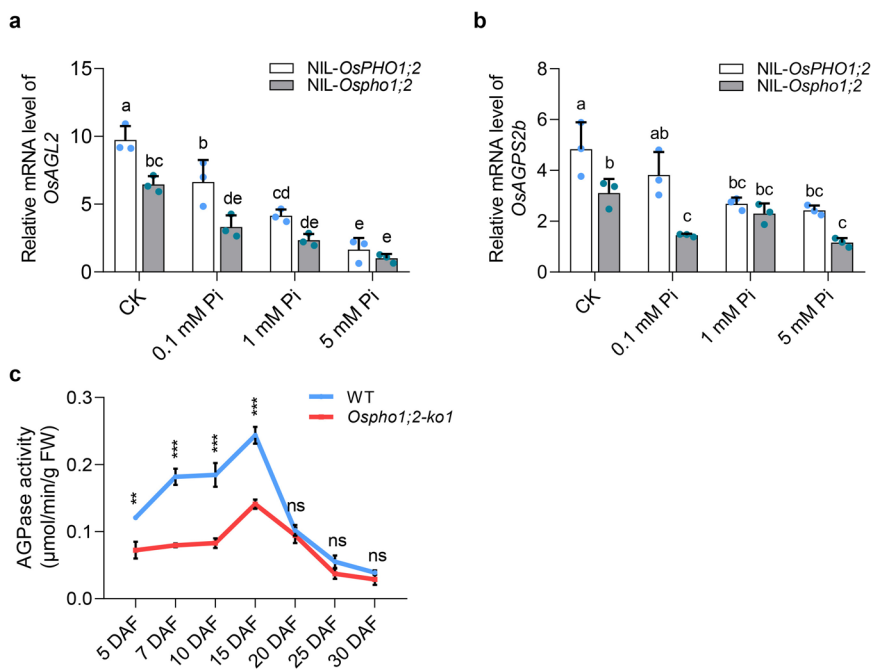
Extended Data Fig. 5 | Immunoelectron microscopy analysis shows that OsPHO1;2 localizes at the plasma membrane. (a-c) Immunoelectron microscopy analysis in the node vascular bundles cells from NIP plants. Samples were immunodetected with the antibody of OsPHO1;2 (b, c) or 1% BSA (a, control). (c) was magnified from blue box area in (b). Scale bars, 500 nm. (d-f) Immunoelectron microscopy analysis in seed nucellar epidermis cells from wild type seeds, and samples were immunodetected with the antibody of OsPHO1;2 (e, f) or 1% BSA (d, control). Scale bars, 200 nm. Black arrowheads denote the immunogold particles in plasma membranes (PM), and positions of cell wall (CW) and cytosol (Cy) are also marked. Images are representatives of at least three independent cells.



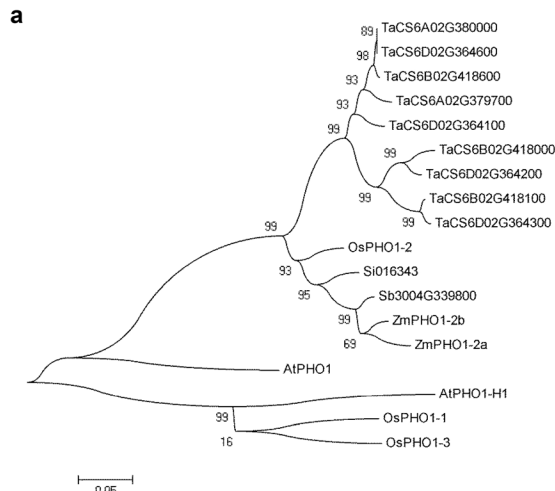
Extended Data Fig. 6 | Transporter activity assay of OsPHO1s under different pH in *Xenopus* oocytes. **a**, Average current-voltage curves for phosphate conductance by OsPHO1;2 and Oospho1;2 in *Xenopus* oocytes. **b**, A detailed exhibition of the current signals at +60 mV and -180 mV from **(a)**. Similar analyses were conducted for OsPHO1;1 (**c** and **d**) and OsPHO1;3 (**e** and **f**). The exact *Xenopus* oocytes number (*n*) was indicated in each graph. Error bars depict means \pm s.e.m (**a**, **c**, **e**). Significant difference was analyzed according to two-tailed Student's *t*-test (**a-f**). *P*-values were calculated through the comparison with Mock pH 5.5. * *P* < 0.05, ** *P* < 0.01, *** *P* < 0.001. OsPHO1;2 pH 5.5 at +60 mV: *P* = 1.60×10^{-7} ; OsPHO1;2 pH 6.5 at +60 mV: *P* = 2.52×10^{-4} ; OsPHO1;2 pH 7.5 at +60 mV: *P* = 1.96×10^{-5} ; OsPHO1;2 pH 5.5 at -180 mV: *P* = 6.65×10^{-6} ; OsPHO1;2 pH 6.5 at -180 mV: *P* = 0.012; OsPHO1;2 pH 7.5 at -180 mV: *P* = 4.23×10^{-3} ; OsPHO1;3 pH 5.5 at -180 mV: *P* = 1.32×10^{-8} ; OsPHO1;3 pH 6.5 at -180 mV: *P* = 2.35×10^{-7} ; OsPHO1;3 pH 7.5 at -180 mV: *P* = 1.40×10^{-9} . For the box-and-whisker plots, the central line, box and whiskers represent the median, IQR and 1.5 times the IQR, respectively (**b**, **d**, **f**).



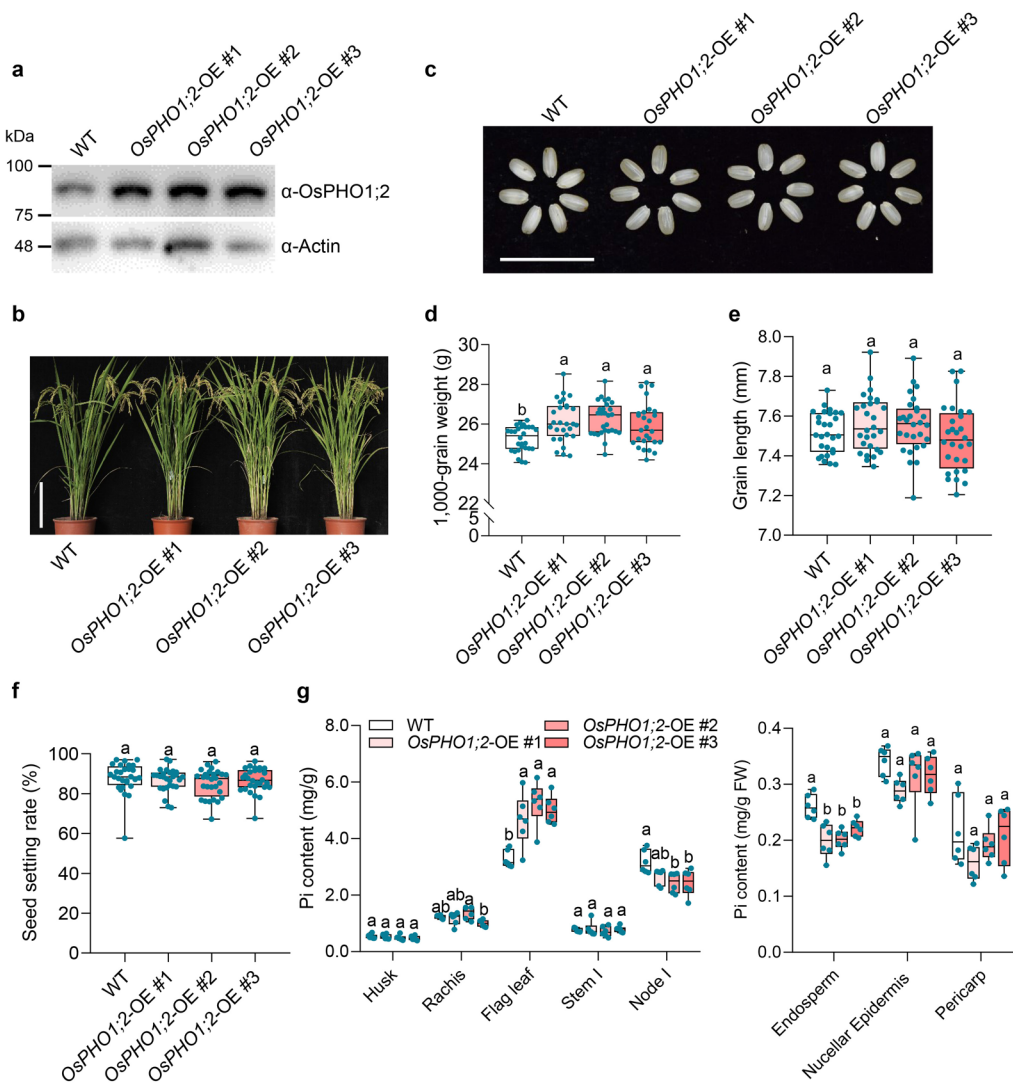
Extended Data Fig. 7 | OsPHO1;2 functions in Pi transfer from root to shoot and reallocation. **(a, b)** Pi contents were measured in root (a) and shoot (b) of seedlings ($n=4$ plants). Germinating seeds were grown for a week in the presence of 1 mM Pi, and then were transferred to Pi-deficient media for the desired period (0–21 d). After 21 days of Pi starvation, plants were transferred to Pi-sufficient conditions for 3 days (21+3 d). Control plants were grown for 25 d in the presence of 1 mM Pi. **(c)** Pairwise comparison of inorganic phosphate (Pi) distribution in different tissues, brown rice, husk, rachis, node I, stem I and flag leaf in NILs and WT/Ospho1;2-ko1 ($n=6$ plants). For the box-and-whisker plots, the central line, box and whiskers represent the median, IQR and 1.5 times the IQR, respectively (a–c). **(d)** Pi distribution in the panicle and leaf tissues of NILs and WT/Ospho1;2-ko1. Values are means \pm s.d. ($n=3$ plants). **(e)** Measurement of Pi contents in different parts of developing seeds (15 DAF). Tissues of pericarp, endosperm and nucellar epidermis were pairwise compared in NIL-OsPHO1;2 and NIL-Ospho1;2. Data are means \pm s.d. ($n=3$ biologically independent samples). P-values were indicated according to two-tailed Student's t-test (a–e).



Extended Data Fig. 8 | Pi accumulation inhibits AGPase production and activity. **a, b**, Relative mRNA levels of *OsAGPL2* (**a**) and *OsAGPS2b* (**b**) in suspension cells of NILs under various Pi treatments. Values are means \pm s.d. ($n=3$ biologically independent samples). $P=1.56 \times 10^{-8}$ (**a**) and $P=1.10 \times 10^{-5}$ (**b**) by one-way ANOVA. Different letters denote significant differences ($P < 0.05$) from Tukey's HSD test. **c**, Measurement of AGPase activity in the WT and *Ospho1;2-ko1* grains from 5 DAF to 30 DAF, values are means \pm s.d. ($n=3$ biologically independent samples). 5 DAF: $P=2.72 \times 10^{-3}$; 7 DAF: $P=1.41 \times 10^{-4}$; 10 DAF: $P=7.56 \times 10^{-4}$; 15 DAF: $P=2.33 \times 10^{-4}$; 20 DAF: $P=0.4068$; 25 DAF: $P=0.0617$; 30 DAF: $P=0.1132$; ** $P < 0.01$, *** $P < 0.001$, ns. not significant, by two-tailed Student's *t*-test.

**b***Zmpho1;2a**Zmpho1;2b*

Extended Data Fig. 9 | Evolutionary analysis of OsPHO1s and its homologs. **a**, Phylogenetic analysis of PHO1 family proteins in rice, *Arabidopsis* and homologs of OsPHO1;2 in other cereal crops including *Zea mays*, *Triticum aestivum*, *Sorghum bicolor* and *Setaria italica*. The tree was built by Mega 5.0. Scale bars, 0.05. **b**, Mutation sites of *Zmpho1;2a* (top) and *Zmpho1;2b* (bottom) generated by CRISPR-Cas9.



Extended Data Fig. 10 | Ectopic overexpression of *OsPHO1;2* significantly enhances grain yield and Pi reallocation. a, Western blot analysis of *OsPHO1;2* protein levels in grains (15 DAF) of the ectopic overexpression lines and WT. Actin was detected as a loading control. Independent experiments were repeated at least 2 times with similar results. **b, c**, Plant morphology (**b**) and seeds phenotype (**c**) of WT and *OsPHO1;2*-OE lines. Scale bars, 20 cm (**b**) and 2 cm (**c**). **(d-f)** Comparison of 1,000-grain weight (**d**), grain length (**e**) and seed setting rate (**f**) between WT and *OsPHO1;2*-OE lines ($n=28$ plants). **(g)** Inorganic phosphate (Pi) distribution in different tissues ($n=6$ plants). Pi was measured in husk, rachis, node I, stem I and flag leaf in WT and *OsPHO1;2*-OE lines (left), and Pi contents in pericarp, endosperm and nucellar epidermis of developing seeds (15 DAF) were also detected (right). $P=3.42 \times 10^{-4}$ (**d**), $P=0.170$ (**e**), $P=0.476$ (**f**), for P -values in (**g**): $P=0.481$ (Husk), $P=0.011$ (Rachis), $P=2.07 \times 10^{-4}$ (Flag leaf), $P=0.803$ (Stem I), $P=0.010$ (Node I), $P=2.40 \times 10^{-4}$ (Endosperm), $P=0.150$ (Nucellar Epidermis), $P=0.167$ (Pericarp), by one-way ANOVA. The different letters denote significant differences ($P < 0.05$) from Tukey's HSD test. For the box-and-whisker plots, the central line, box and whiskers represent the median, IQR and 1.5 times the IQR, respectively (**d-g**).

Reporting Summary

Nature Research wishes to improve the reproducibility of the work that we publish. This form provides structure for consistency and transparency in reporting. For further information on Nature Research policies, see [Authors & Referees](#) and the [Editorial Policy Checklist](#).

Statistics

For all statistical analyses, confirm that the following items are present in the figure legend, table legend, main text, or Methods section.

n/a Confirmed

- The exact sample size (n) for each experimental group/condition, given as a discrete number and unit of measurement
- A statement on whether measurements were taken from distinct samples or whether the same sample was measured repeatedly
- The statistical test(s) used AND whether they are one- or two-sided
Only common tests should be described solely by name; describe more complex techniques in the Methods section.
- A description of all covariates tested
- A description of any assumptions or corrections, such as tests of normality and adjustment for multiple comparisons
- A full description of the statistical parameters including central tendency (e.g. means) or other basic estimates (e.g. regression coefficient) AND variation (e.g. standard deviation) or associated estimates of uncertainty (e.g. confidence intervals)
- For null hypothesis testing, the test statistic (e.g. F , t , r) with confidence intervals, effect sizes, degrees of freedom and P value noted
Give P values as exact values whenever suitable.
- For Bayesian analysis, information on the choice of priors and Markov chain Monte Carlo settings
- For hierarchical and complex designs, identification of the appropriate level for tests and full reporting of outcomes
- Estimates of effect sizes (e.g. Cohen's d , Pearson's r), indicating how they were calculated

Our web collection on [statistics for biologists](#) contains articles on many of the points above.

Software and code

Policy information about [availability of computer code](#)

Data collection

Fluorescence signals were detected using a confocal microscope (Olympus Fluoview FV1000). The whole-cell patch-clamp recordings were performed using an Axopatch-200B patch-clamp setup (Axon Instruments, CA, USA) with a Digitata1550 digitizer (Axon Instruments, CA, USA). 31P NMR data was acquired according to MestReNova software version 6.1.1-6384. Total P μXRF images were obtained from M4 Tornado ESPRIT.

Data analysis

Data were analyzed by GraphPad Prism 8.0 and Excel 2013 to perform two-tailed Student's t-test, and Minitab 18 software to perform One-way ANOVA followed by Tukey-test for multiple comparisons. And pClamp10.7 software (Axon Instruments, CA, USA) was used for data acquisition and analysis of patch-clamp result.

For manuscripts utilizing custom algorithms or software that are central to the research but not yet described in published literature, software must be made available to editors/reviewers. We strongly encourage code deposition in a community repository (e.g. GitHub). See the Nature Research [guidelines for submitting code & software](#) for further information.

Data

Policy information about [availability of data](#)

All manuscripts must include a [data availability statement](#). This statement should provide the following information, where applicable:

- Accession codes, unique identifiers, or web links for publicly available datasets
- A list of figures that have associated raw data
- A description of any restrictions on data availability

The entire RNA-Seq datasets have been deposited in the NCBI Gene Expression Omnibus (GEO) under accession number: GSE149101.

Field-specific reporting

Please select the one below that is the best fit for your research. If you are not sure, read the appropriate sections before making your selection.

- Life sciences Behavioural & social sciences Ecological, evolutionary & environmental sciences

For a reference copy of the document with all sections, see nature.com/documents/nr-reporting-summary-flat.pdf

Life sciences study design

All studies must disclose on these points even when the disclosure is negative.

Sample size	Samples size for each experiment is indicated in the legends. Required experimental sample size was chosen based on our previous experience in the lab. Each experiment contains at least three replicates. No statistical methods were used to predetermine sample size.
Data exclusions	No data were excluded.
Replication	All experiments were successfully repeated independently at least two times, and the number of independent experiments or biological replicates is indicated in the figure legends.
Randomization	Plants, cells, and cell cultures were randomly assigned to the treatment and control groups with no formal randomization techniques in this study.
Blinding	No blinding was used in this study due to all genotypes in particular transgenic materials should be independently labeled and stored to avoid contamination and thus phenotypes were measured as mentioned in Method section.

Behavioural & social sciences study design

All studies must disclose on these points even when the disclosure is negative.

Study description	Briefly describe the study type including whether data are quantitative, qualitative, or mixed-methods (e.g. qualitative cross-sectional, quantitative experimental, mixed-methods case study).
Research sample	State the research sample (e.g. Harvard university undergraduates, villagers in rural India) and provide relevant demographic information (e.g. age, sex) and indicate whether the sample is representative. Provide a rationale for the study sample chosen. For studies involving existing datasets, please describe the dataset and source.
Sampling strategy	Describe the sampling procedure (e.g. random, snowball, stratified, convenience). Describe the statistical methods that were used to predetermine sample size OR if no sample-size calculation was performed, describe how sample sizes were chosen and provide a rationale for why these sample sizes are sufficient. For qualitative data, please indicate whether data saturation was considered, and what criteria were used to decide that no further sampling was needed.
Data collection	Provide details about the data collection procedure, including the instruments or devices used to record the data (e.g. pen and paper, computer, eye tracker, video or audio equipment) whether anyone was present besides the participant(s) and the researcher, and whether the researcher was blind to experimental condition and/or the study hypothesis during data collection.
Timing	Indicate the start and stop dates of data collection. If there is a gap between collection periods, state the dates for each sample cohort.
Data exclusions	If no data were excluded from the analyses, state so OR if data were excluded, provide the exact number of exclusions and the rationale behind them, indicating whether exclusion criteria were pre-established.
Non-participation	State how many participants dropped out/declined participation and the reason(s) given OR provide response rate OR state that no participants dropped out/declined participation.
Randomization	If participants were not allocated into experimental groups, state so OR describe how participants were allocated to groups, and if allocation was not random, describe how covariates were controlled.

Ecological, evolutionary & environmental sciences study design

All studies must disclose on these points even when the disclosure is negative.

Study description	Briefly describe the study. For quantitative data include treatment factors and interactions, design structure (e.g. factorial, nested, hierarchical), nature and number of experimental units and replicates.
Research sample	Describe the research sample (e.g. a group of tagged <i>Passer domesticus</i> , all <i>Stenocereus thurberi</i> within Organ Pipe Cactus National Monument), and provide a rationale for the sample choice. When relevant, describe the organism taxa, source, sex, age range and

Sampling strategy	Note the sampling procedure. Describe the statistical methods that were used to predetermine sample size OR if no sample-size calculation was performed, describe how sample sizes were chosen and provide a rationale for why these sample sizes are sufficient.
Data collection	Describe the data collection procedure, including who recorded the data and how.
Timing and spatial scale	Indicate the start and stop dates of data collection, noting the frequency and periodicity of sampling and providing a rationale for these choices. If there is a gap between collection periods, state the dates for each sample cohort. Specify the spatial scale from which the data are taken
Data exclusions	If no data were excluded from the analyses, state so OR if data were excluded, describe the exclusions and the rationale behind them, indicating whether exclusion criteria were pre-established.
Reproducibility	Describe the measures taken to verify the reproducibility of experimental findings. For each experiment, note whether any attempts to repeat the experiment failed OR state that all attempts to repeat the experiment were successful.
Randomization	Describe how samples/organisms/participants were allocated into groups. If allocation was not random, describe how covariates were controlled. If this is not relevant to your study, explain why.
Blinding	Describe the extent of blinding used during data acquisition and analysis. If blinding was not possible, describe why OR explain why blinding was not relevant to your study.

Did the study involve field work? Yes No

Field work, collection and transport

Field conditions	Describe the study conditions for field work, providing relevant parameters (e.g. temperature, rainfall).
Location	State the location of the sampling or experiment, providing relevant parameters (e.g. latitude and longitude, elevation, water depth).
Access and import/export	Describe the efforts you have made to access habitats and to collect and import/export your samples in a responsible manner and in compliance with local, national and international laws, noting any permits that were obtained (give the name of the issuing authority, the date of issue, and any identifying information).
Disturbance	Describe any disturbance caused by the study and how it was minimized.

Reporting for specific materials, systems and methods

We require information from authors about some types of materials, experimental systems and methods used in many studies. Here, indicate whether each material, system or method listed is relevant to your study. If you are not sure if a list item applies to your research, read the appropriate section before selecting a response.

Materials & experimental systems		Methods	
n/a	Involved in the study	n/a	Involved in the study
<input type="checkbox"/>	<input checked="" type="checkbox"/> Antibodies	<input type="checkbox"/>	<input checked="" type="checkbox"/> ChIP-seq
<input type="checkbox"/>	<input checked="" type="checkbox"/> Eukaryotic cell lines	<input type="checkbox"/>	<input checked="" type="checkbox"/> Flow cytometry
<input checked="" type="checkbox"/>	<input type="checkbox"/> Palaeontology	<input type="checkbox"/>	<input checked="" type="checkbox"/> MRI-based neuroimaging
<input type="checkbox"/>	<input checked="" type="checkbox"/> Animals and other organisms		
<input checked="" type="checkbox"/>	<input type="checkbox"/> Human research participants		
<input checked="" type="checkbox"/>	<input type="checkbox"/> Clinical data		

Antibodies

Antibodies used	We used three custom-made and six commercial antibodies in the study, including Rabbit polyclonal anti-OsPHO1;2 (Abmart, custom made, 1:500 for Western blot and 1:100 for immunofluorescence assay and 1:20 for immunogold labelling analysis), Rabbit polyclonal anti-OsAGPL2 (Abmart, custom made, 1:1500), Rabbit polyclonal anti-OsAGPS2b (Abmart, custom made, 1:1500), Mouse monoclonal anti-Actin (CWBIO, CW0264M, 1:5000), Rabbit polyclonal anti-Bt2 (Agrisera, AS111739, 1:2500), Rabbit polyclonal anti-GUS (Abcam, Ab50148, 1:500), Goat anti-Rabbit IgG (H+L), Alexa Fluor 546 (Thermo Fisher Scientific, A-11010, 1:500), Goat Anti-Rabbit IgG HRP (Abbkine, A21040, 1:5000), Goat Anti-Mouse IgG HRP (BIORAD, 1706516, 1:5000), Anti-Rabbit IgG (whole molecule)-Gold antibody (Sigma, G7402, 1:30).
Validation	Each antibody has been validated for the application used in the manuscript. The validation information of six commercial antibodies is listed as follows: Mouse monoclonal anti-Actin (validated for WB in Arabidopsis and rice), Rabbit polyclonal anti-Bt2 (validated for WB in Arabidopsis, maize and barely), Rabbit polyclonal anti-GUS (validated for WB and immunohistochemistry in plants), Goat anti-Rabbit IgG (H+L), Alexa Fluor 546 (validated for WB and IHC in many organisms including rice), Goat Anti-Rabbit

IgG HRP (validated for WB and IHC in many organisms including rice). The custom-made antibody Rabbit polyclonal anti-OsAGPL2 was validated for WB and IHC in rice, and the custom-made antibodies Rabbit polyclonal anti-OsAGPL2 and Rabbit polyclonal anti-OsAGPS2b were validated for WB in rice. Positive and negative controls were included in all experiments. The information of custom-made antibodies are mentioned in the method part of the manuscript and their usage can be found in Fig.2b-d, Fig.4b,4e, Fig.6c, Extended Data Fig. 4b, 4d, Extended Data Fig.5a-f, Extended Data Fig.10a. The information for Rabbit polyclonal anti-OsAGPL2 (Abmart, custom made) and Rabbit polyclonal anti-OsAGPS2b (Abmart, custom made) can also be found in a published paper with doi:10.1016/j.plantsci.2016.05.010.

Eukaryotic cell lines

Policy information about [cell lines](#)

Cell line source(s)	HEK293T cell line was provided by the Cell Culture Facility, University of California, Berkeley, originally obtained from VA Seaman's hospital.
Authentication	The cell line was verified using short tandem repeat profiling at the UCB DNA Sequencing Facility.
Mycoplasma contamination	The cell line was tested for Mycoplasma contamination.
Commonly misidentified lines (See ICLAC register)	The cell line is not a commonly misidentified line according to the ICLAC register.

Palaeontology

Specimen provenance	Provide provenance information for specimens and describe permits that were obtained for the work (including the name of the issuing authority, the date of issue, and any identifying information).
Specimen deposition	Indicate where the specimens have been deposited to permit free access by other researchers.
Dating methods	If new dates are provided, describe how they were obtained (e.g. collection, storage, sample pretreatment and measurement), where they were obtained (i.e. lab name), the calibration program and the protocol for quality assurance OR state that no new dates are provided.

Tick this box to confirm that the raw and calibrated dates are available in the paper or in Supplementary Information.

Animals and other organisms

Policy information about [studies involving animals; ARRIVE guidelines](#) recommended for reporting animal research

Laboratory animals	This study used Xenopus oocytes that were produced and provided by the Cell Culture Facility, University of California, Berkeley. The Xenopus oocytes were used to detect the patch-clamping transporter activities in the Berkeley laboratory as usual, and all Xenopus oocyte experiments were completed in accordance with animal research ethics regulations.
Wild animals	This study did not involve wild animals.
Field-collected samples	Plants were grown at the experimental stations in Shanghai for the summer season, or Lingshui for the winter season (Hainan Island, southern China) under natural conditions for adult plant growth and seed production. Most plant related samples were collected in the field of Shanghai or Lingshui.
Ethics oversight	We applied well-recognized protocols for all the experiments, and provided the details in the method part for checking.

Note that full information on the approval of the study protocol must also be provided in the manuscript.

Human research participants

Policy information about [studies involving human research participants](#)

Population characteristics	Describe the covariate-relevant population characteristics of the human research participants (e.g. age, gender, genotypic information, past and current diagnosis and treatment categories). If you filled out the behavioural & social sciences study design questions and have nothing to add here, write "See above."
Recruitment	Describe how participants were recruited. Outline any potential self-selection bias or other biases that may be present and how these are likely to impact results.
Ethics oversight	Identify the organization(s) that approved the study protocol.

Note that full information on the approval of the study protocol must also be provided in the manuscript.

Clinical data

Policy information about [clinical studies](#)

All manuscripts should comply with the ICMJE [guidelines for publication of clinical research](#) and a completed [CONSORT checklist](#) must be included with all submissions.

Clinical trial registration

Provide the trial registration number from ClinicalTrials.gov or an equivalent agency.

Study protocol

Note where the full trial protocol can be accessed OR if not available, explain why.

Data collection

Describe the settings and locales of data collection, noting the time periods of recruitment and data collection.

Outcomes

Describe how you pre-defined primary and secondary outcome measures and how you assessed these measures.

ChIP-seq

Data deposition

Confirm that both raw and final processed data have been deposited in a public database such as [GEO](#).

Confirm that you have deposited or provided access to graph files (e.g. BED files) for the called peaks.

Data access links

May remain private before publication.

For "Initial submission" or "Revised version" documents, provide reviewer access links. For your "Final submission" document, provide a link to the deposited data.

Files in database submission

Provide a list of all files available in the database submission.

Genome browser session (e.g. [UCSC](#))

Provide a link to an anonymized genome browser session for "Initial submission" and "Revised version" documents only, to enable peer review. Write "no longer applicable" for "Final submission" documents.

Methodology

Replicates

Describe the experimental replicates, specifying number, type and replicate agreement.

Sequencing depth

Describe the sequencing depth for each experiment, providing the total number of reads, uniquely mapped reads, length of reads and whether they were paired- or single-end.

Antibodies

Describe the antibodies used for the ChIP-seq experiments; as applicable, provide supplier name, catalog number, clone name, and lot number.

Peak calling parameters

Specify the command line program and parameters used for read mapping and peak calling, including the ChIP, control and index files used.

Data quality

Describe the methods used to ensure data quality in full detail, including how many peaks are at FDR 5% and above 5-fold enrichment.

Software

Describe the software used to collect and analyze the ChIP-seq data. For custom code that has been deposited into a community repository, provide accession details.

Flow Cytometry

Plots

Confirm that:

- The axis labels state the marker and fluorochrome used (e.g. CD4-FITC).
- The axis scales are clearly visible. Include numbers along axes only for bottom left plot of group (a 'group' is an analysis of identical markers).
- All plots are contour plots with outliers or pseudocolor plots.
- A numerical value for number of cells or percentage (with statistics) is provided.

Methodology

Sample preparation

Describe the sample preparation, detailing the biological source of the cells and any tissue processing steps used.

Instrument

Identify the instrument used for data collection, specifying make and model number.

Software

Describe the software used to collect and analyze the flow cytometry data. For custom code that has been deposited into a community repository, provide accession details.

Cell population abundance

Describe the abundance of the relevant cell populations within post-sort fractions, providing details on the purity of the samples and how it was determined.

Gating strategy

Describe the gating strategy used for all relevant experiments, specifying the preliminary FSC/SSC gates of the starting cell population, indicating where boundaries between "positive" and "negative" staining cell populations are defined.

Tick this box to confirm that a figure exemplifying the gating strategy is provided in the Supplementary Information.

Magnetic resonance imaging

Experimental design

Design type

Indicate task or resting state; event-related or block design.

Design specifications

Specify the number of blocks, trials or experimental units per session and/or subject, and specify the length of each trial or block (if trials are blocked) and interval between trials.

Behavioral performance measures

State number and/or type of variables recorded (e.g. correct button press, response time) and what statistics were used to establish that the subjects were performing the task as expected (e.g. mean, range, and/or standard deviation across subjects).

Acquisition

Imaging type(s)

Specify: functional, structural, diffusion, perfusion.

Field strength

Specify in Tesla

Sequence & imaging parameters

Specify the pulse sequence type (gradient echo, spin echo, etc.), imaging type (EPI, spiral, etc.), field of view, matrix size, slice thickness, orientation and TE/TR/flip angle.

Area of acquisition

State whether a whole brain scan was used OR define the area of acquisition, describing how the region was determined.

Diffusion MRI

Used

Not used

Preprocessing

Preprocessing software

Provide detail on software version and revision number and on specific parameters (model/functions, brain extraction, segmentation, smoothing kernel size, etc.).

Normalization

If data were normalized/standardized, describe the approach(es): specify linear or non-linear and define image types used for transformation OR indicate that data were not normalized and explain rationale for lack of normalization.

Normalization template

Describe the template used for normalization/transformation, specifying subject space or group standardized space (e.g. original Talairach, MNI305, ICBM152) OR indicate that the data were not normalized.

Noise and artifact removal

Describe your procedure(s) for artifact and structured noise removal, specifying motion parameters, tissue signals and physiological signals (heart rate, respiration).

Volume censoring

Define your software and/or method and criteria for volume censoring, and state the extent of such censoring.

Statistical modeling & inference

Model type and settings

Specify type (mass univariate, multivariate, RSA, predictive, etc.) and describe essential details of the model at the first and second levels (e.g. fixed, random or mixed effects; drift or auto-correlation).

Effect(s) tested

Define precise effect in terms of the task or stimulus conditions instead of psychological concepts and indicate whether ANOVA or factorial designs were used.

Specify type of analysis: Whole brain ROI-based Both

Statistic type for inference
(See [Eklund et al. 2016](#))

Specify voxel-wise or cluster-wise and report all relevant parameters for cluster-wise methods.

Correction

Describe the type of correction and how it is obtained for multiple comparisons (e.g. FWE, FDR, permutation or Monte Carlo).

Models & analysis

n/a Involved in the study

Functional and/or effective connectivity

Graph analysis

Multivariate modeling or predictive analysis

Functional and/or effective connectivity

Report the measures of dependence used and the model details (e.g. Pearson correlation, partial correlation, mutual information).

Graph analysis

Report the dependent variable and connectivity measure, specifying weighted graph or binarized graph, subject- or group-level, and the global and/or node summaries used (e.g. clustering coefficient, efficiency, etc.).

Multivariate modeling and predictive analysis

Specify independent variables, features extraction and dimension reduction, model, training and evaluation metrics.